Acclimation strategies of the green alga *Chlorella vulgaris* to different light regimes revealed by physiologic and comparative proteomic analyses

Michela Cecchin[1], Jovan Simicevic[2], Louise Chaput[2], Manuel Hernandez[2], Laura Girolomoni[1], Stefano Cazzaniga[1], Claire Remacle[3], Julia Hoeng[2], Nikolai V. Ivanov[2], Bjoern Titz[2], Matteo Ballottari[1*]

[1]*Dipartimento di Biotecnologie, Università di Verona, Strada Le Grazie 15, 37134 Verona, Italy*

[2]*PMI R&D, Philip Morris Products S.A., Quai Jeanrenaud 5, 2000 Neuchâtel, Switzerland*

[3]*Genetics and Physiology of Microalgae, InBios/Phytosystems Research Unit, University of Liège, 4000 Liège, Belgium*

**Address for correspondence: Matteo Ballottari, Dipartimento di Biotecnologie, Università di Verona, Strada le Grazie 15, 37134 Verona, Italy; Tel: +390458027807; E-mail: matteo.ballottari@univr.it*

Number of Tables: 2

Number of Figures: 6

Word count: 7993

Supplementary data: Table S1-S5, Figure S1-S10, Dataset S1-S3

Running title: *Chlorella vulgaris* acclimation strategies to different irradiances

HIGHLIGHT

Acclimation to different irradiances was investigated in the fast-growing green alga *Chlorella vulgaris*, focusing on photosynthetic and mitochondrial activities and identifying differentially expressed proteins including transcription factors and signaling components.

ABSTRACT

Acclimation to different light regimes is at the base of survival for photosynthetic organisms, regardless of their evolutionary origin. Previous research efforts largely focused on acclimation events occurring at the level of photosynthetic apparatus and often highlighted species-specific mechanisms. Here, we investigated the consequences of acclimation to different irradiances in *Chlorella vulgaris*, a green alga that is one of the most promising species for industrial application, focusing on both photosynthetic and mitochondrial activities. Moreover, proteomic analysis of cells acclimated to high light (HL) or low light (LL) allowed identification of the main targets of acclimation in terms of differentially expressed proteins. The results obtained demonstrate photosynthetic adaptation to HL vs. LL that were only partially consistent with previous findings in *Chlamydomonas reinhardtii,* a model organism for green algae, but in many cases similar to vascular plant acclimation events. Increased mitochondrial respiration measured in HL-acclimated cells mainly relied on alternative oxidative pathway dissipating the excessive reducing power produced due to enhanced carbon flow. Finally, proteins involved in cell metabolism, intracellular transport, gene expression, and signaling—including an heliorhodopsin homolog—were identified as strongly differentially expressed in HL vs. LL, suggesting their key roles in acclimation to different light regimes.

KEYWORDS: abiotic stress, carotenoids, *Chlorella vulgaris,* microalgae, photosynthesis, proteomics

ABBREVIATIONS: ABC1K1, activity of bc1 complex kinase 1; ACS, acetyl-CoA synthase; AOX, alternative oxidase; CBB, Calvin-Benson-Bassham; Chl, chlorophyll; DBMIB, 2,5-dibromo-6-isopropyl-3-methyl-1,4-benzoquinone; DCMU, 3-(3,4-dichlorophenyl)-1,1-dimethylurea; ECS, electrochemical shift; ETR, electron transport rate; FDR, false discovery rate; GO, Gene Ontology; HL, high light; LHCSR, light harvesting complex stress related; LL, low light; LRR, leucin-rich repeat; NPQ, non-photochemical quenching; PAT, phosphate acetyltransferase; Pmax, Pmax, maximum light dependent net oxygen evolution rate; ΦPSII, maximum photochemical efficiency of PSII; qL, fraction of open reaction centers in PSII; SHAM, salicylhydroxamic acid; TCA, tricarboxylic acid

INTRODUCTION

Photosynthesis is the metabolic process by which light energy is harvested and converted into chemical energy to fix CO2 into organic molecules, as sugars. In eukaryotic photosynthetic organisms, PSI and PSII are the pigment-binding complexes located in the thylakoid membranes that harvest photons and use the excitation energy to generate electron transport from water to NADPH; this electron transport is coupled with proton transport that generates an electrochemical gradient across thylakoid membranes, enabling ATP biosynthesis. The Calvin-Benson-Bassham (CBB) cycle is the subsequent metabolic process occurring in the stroma where ATP and NADPH are consumed to fix CO_2. Among photosynthetic organisms, unicellular microalgae raised interest due to the possibility to cultivate them in artificial systems in industrial environments to exploit their photosynthetic capability to fix CO_2 into bioproducts of interest including food additives, proteins, lipids, antioxidants, biostimulants, and possibly biofuels (Camacho, Macedo, & Malcata, 2019; Chisti, 2008; Koyande et al., 2019; Rani et al., 2021; Rosch, Rossmann, & Weickert, 2019). Several microalgae species were considered for industrial application, such as *Chlorella* species, which are characterized by fast growth and high resistance to biotic and abiotic stresses (Ananyev, Gates, Kaplan, & Dismukes, 2017; Arriola et al., 2018; Blanc et al., 2010; Juneja, Chaplen, & Murthy, 2016; Niccolai, Zittelli, Rodolfi, Biondi, & Tredici, 2019; Sarayloo et al., 2017; Sathasivam, Radhakrishnan, Hashem, & Abd Allah, 2019; Treves et al., 2016; Zuniga et al., 2016). Indeed, some *Chlorella* species are already in the market as food and feed supplements, (Lum, Kim, & Lei, 2013). *Chlorella vulgaris* is one of the few microalgae species approved as novel food for human consumption (Bernaerts, Gheysen, Foubert, Hendrickx, & Van Loey, 2019).

Microalgae photosynthetic efficiency and productivity are strictly dependent on their capacity to adapt and acclimate to the conditions of growth where irradiance, temperature, CO_2, and nutrient availability are among the key parameters influencing cell growth (Vecchi, Barera, Bassi, & Dall'Osto, 2020). The consequences of growing at different light intensities were deeply investigated in several microalgae species in previous works: the chlorophyll (Chl) content per cell and chlorophyll-to-carotenoid ratio are generally reduced for different microalgae species grown in high light (HL) compared to cells acclimated to low light (LL) (Bonente, Pippa, Castellano, Bassi, & Ballottari, 2012; Simionato et al., 2011). Moreover, the light-harvesting capacity, or functional “antenna size” of PSII, measured from Chl a fluorescence induction curve in presence of PSII inhibitor, or estimated from Chl a/b ratio, were reported to be reduced in several species such as *Dunaliella salina*, *Dunaliella viridis* (Gordillo, Jiménez, Chavarría, & Xavier Niell, 2001; Smith et al., 1990), and diatoms (Lavaud, Rousseau, & Etienne, 2004) upon acclimation to HL. Differently, in the case of the model organism for green algae, *Chlamydomonas reinhardtii*, and in *Nannochloropsis gaditana*, similar functional antenna sizes were measured in cells grown at low or high irradiance (Bonente et al., 2012; Simionato et al., 2011). Cells grown in HL conditions are also generally characterized by an increased capability to induce photoprotective mechanisms as thermal dissipation of the light absorbed (or non-photochemical quenching, NPQ) as reported in the case of *C. reinhardtii* (Peers et al., 2009), diatoms (Lepetit et al., 2012; Zhu & Green, 2010), and *Nannochloropsis* (Chukhutsina, Fristedt, Morosinotto, & Croce, 2017). Regulation of CBB enzyme

accumulation and activity was also reported to have a key role in acclimation to HL, with a general increased capacity for carbon fixation in cells acclimated to high irradiance (Bonente et al., 2012). It is important to note that in eukaryotic photosynthetic organisms as microalgae, photosynthetic metabolism is coupled with mitochondrial metabolism (Bailleul et al., 2015; Johnson & Alric, 2013; Uhmeyer, Cecchin, Ballottari, & Wobbe, 2017), where organic molecules are oxidized to CO_2, producing reducing power that can be used to produce ATP. The mitochondrial electron transport chain, also known as the cytochrome pathway, includes an ATP synthase complex (complex V) and four oxidoreductase complexes that oxidize the reducing power and produce ATP by an electrochemical gradient that is formed across the membrane. In addition, an alternative oxidase (AOX) might directly couple ubiquinol oxidation with the reduction of O_2 to H_2O, serving as an alternative route that bypasses the electron transport chain, thus dramatically reducing the energy (ATP) yield. In plants, AOX was reported to have a role in respiratory chain protection mechanisms by preventing saturation of the electron carriers (Boekema & Braun, 2007; Vanlerberghe, 2013). An additional alternative oxidase, called PTOX (Plastid Terminal Oxidase), was characterized in the chloroplast being involved in chlororespiration transferring electrons from plastoquinone pool to oxygen (Arnon, Tsujimoto, & Tang, 1981; Bennoun, 1982; Kedem, Milrad, Kaplan, & Yacoby, 2021; Rumeau, Peltier, & Cournac, 2007). PTOX activity has been previously reported to prevent electron transport chain saturation (Kedem et al., 2021; Niyogi, 2000), but at same time its activity has been shown to be crucial for carotenogenesis (Li, Sommerfeld, Chen, & Hu, 2010; Shahbazi, Gilbert, Labouré, & Kuntz, 2007). It is important to note that crosstalk between plastids and mitochondria was proposed in several microalgae species, where the activity of one of the two organelles influences the redox state of the other (Bailleul et al., 2015; Burlacot, Peltier, & Li-Beisson, 2019; Cecchin, Paloschi, et al., 2021; Uhmeyer et al., 2017). In this context, the impact of mitochondrial activity in HL acclimation in microalgae has not been fully elucidated.

In this work, we investigated the consequences of acclimation at high or low irradiances in *C. vulgaris* with a focus on photosynthetic and mitochondrial activities. Moreover, proteomic analysis of cells acclimated to HL or LL allowed us to identify the main target of acclimation in terms of variable protein expression, suggesting possible targets for future biotechnological modifications.

MATERIALS AND METHODS

Chlorella vulgaris cultivation. *C. vulgaris 211/11P* strain (Cecchin et al., 2019) was obtained from the Culture Collection of Algae at Goettingen University. LL and HL acclimation was induced by growing *C. vulgaris* cells in photoautotrophy in BG-11 medium (Allen & Stanier, 1968) at 25°C (Serra-Maia, Bernard, Goncalves, Bensalem, & Lopes, 2016) in flasks at 70 µmol m^{-2} s^{-1} or 850 µmol m^{-2} s^{-1} white light irradiation. No additional inorganic carbon was supplied, and a rotative shaker (150 rpm) was used to prevent cell sedimentation and induce gas exchange. The cell cultures were exposed to light from the bottom of the flask and the light path (from the bottom to the top of the culture) was 1 cm. The light gradient at which the cells were exposed during growth was calculated from the pigment concentration in the cultures and their transmittance spectra (Fig. S1).

The cells grown in LL and HL conditions were refreshed at least ten times diluting the cells to pre-exponential phase before the experiments. Sampling for physiologic measurements and for proteomic analysis were done during exponential phase for at least three different biological replicates grown at the same time. At the end of the growth curve the dry weight determination was performed: cell culture was harvested by centrifugation at 4500g for 5 min at 20°C then freeze-dried for 48h and then net dry weight was calculated. Protein concentration was determined by bicinchoninic acid (BCA) protein assay (Thermo Fisher Scientific; Waltham, MA, USA).

Photosynthetic parameters. Photosynthetic parameters as maximum photochemical efficiency of PSII (ΦPSII), fraction of open reaction centers in PSII (qL), electron transport rate (ETR), and NPQ were measured with a DUAL-PAM-100 fluorometer (Heinz–Walz; Effeltrich, Germany) at room temperature in a 1 × 1-cm cuvette mixed by magnetic stirring (Baker, 2008). PSII functional antenna size was estimated from the fast Chl fluorescence induction kinetics with a DUAL-PAM-100 fluorometer after induction with a red light of 11-μmol photons m^{-2} s^{-1} on dark-adapted cells (~2 × 10^6 cells/mL) incubated with 50 μM DCMU (3-(3,4-dichlorophenyl)-1,1-dimethylurea). The reciprocal of time corresponding to two-thirds of the fluorescence rise (τ2/3) was taken as a measure of the PSII functional antenna size (Malkin, Armond, Mooney, & Fork, 1981). The 77K fluorescence emission spectra were acquired with a charge-coupled device spectrophotometer (JBeamBio; La Rochelle, France) as previously described (Allorent et al., 2013). State transitions were measured on whole cells induced to state 1 or state 2 as previously described (Fleischmann et al., 1999). The reduction rate of NAD(P)H was determined with the NADPH/9-AA module of the DUAL-PAM 101 using 1400 μmol photons m^{-2} s^{-1} as actinic light (Cecchin, Paloschi, et al., 2021; Schreiber & Klughammer, 2009): NAD(P)H formation was analyzed following the fluorescence emission in the 420-580 nm range upon excitation at 365 nm. Proton motive force upon exposure to different light intensities was measured as the electrochemical shift (ECS) with MultispeQ v2.0 (PhotosynQ; East Lansing, MI, USA) according to (Kuhlgert et al., 2016) and normalized to the Chl content of the sample. PSI functional antenna size was measured in thylakoids (300 μg/mL of Chl concentration) obtained from acclimated cells with the DUAL-PAM-100 in presence of DCMU and DBMIB (2,5-dibromo-6-isopropyl-3-methyl-1,4-benzoquinone) following transient absorption at 830 nm upon exposure to actinic light (11-μmol photons m^{-2} s^{-1}). Maximum P700 activity was measured as described in (Cecchin, Paloschi, et al., 2021).

Pigment analysis. Pigments were extracted with 100% DMSO at 60°C in dark conditions and measured with a JASCO V-550 UV/VIS spectrophotometer (Halifax, NS, Canada). HPLC analysis was performed as described in (Perozeni et al., 2020).

Oxygen evolution and mitochondrial respiration. Oxygen evolution rates and mitochondrial respiration were measured at 25°C with a Clark-type O_2 electrode (Hansatech; King's Lynn, Norfolk, UK), as described previously (Cecchin, Paloschi, et al., 2021). The individual contributions of the alternative and cytochrome (complex III) pathways in mitochondrial respiration were estimated by inhibiting them with SHAM (salicylhydroxamic acid) and myxothiazol inhibitors, respectively: the concentration adopted, 2mM and 5μM respectively, were chosen according to previous results in the same species (Cecchin, Paloschi, et al., 2021)

Respiration was first measured in the absence of inhibitors (total dark respiration) before alternative respiration was inhibited by adding SHAM. Cytochrome-dependent respiration was then inhibited using myxothiazol, and residual respiration was determined in relation to the uninhibited state. The contribution of alternative respiration was determined by reversing the order of inhibitor addition (myxothiazol followed by SHAM) (Bailleul et al., 2015).

SDS-PAGE and western blot analysis. SDS-PAGE and immunoblotting were performed as described in (Bonente et al., 2011). The following antibodies, α-RbcL AS03 037, α-PsaA AS06 172 and α-PsbC (CP43) AS11 1787 were obtained from Agrisera company (Agrisera, Vannas, Sweden). Samples were compared only when loaded on the same gel.

Subcellular localization prediction. Subcellular localization prediction was performed with the PredAlgo tool (Tardif et al., 2012).

Proteomic analysis. *C. vulgaris* sample cell disruption was performed utilizing a CP02 cryoPREP Automated Dry Pulverizer (Covaris, Woburn, MA, USA); total protein was extracted with the ReadyPrep Protein Extraction Kit (Bio-Rad; Hercules, CA, USA) and a Tissue Lyser II system (Qiagen; Hilden, Germany). Samples were then centrifuged for 5 min at 16,000 g, and the supernatants (400 µL) were transferred to new tubes. Proteins were precipitated by separately adding four volumes of acetone to one volume of each protein extract, vortexed, and precipitated overnight at -20°C. The next day, individual tubes were centrifuged for 30 min at 10°C at 16,000 g. The supernatants were removed, then one volume of pre-chilled acetone was added to each tube. The tubes were centrifuged one more time, and the previous step was repeated. The supernatants were again discarded, and the protein pellets were dried using a speed vacuum for <1 min. The dried protein pellets were separately resuspended in 200 µL of resuspension buffer (1 M urea, 0.5 M triethylammonium bicarbonate [TEAB], 0.1% SDS), vortexed, and centrifuged at 16,000 g for 25 s. The samples were sonicated for 30 s then centrifuged for 1 min at 16,000 g before the supernatants were collected. Protein amounts were measured with the Quick Start Bradford Protein Assay (Bio-Rad) utilizing bovine serum albumin as the standard. Protein concentrations were normalized to 1 µg/µL in resuspension buffer in a final volume of 30 µL. Protein reduction, alkylation, digestion, and purification was performed utilizing the Preomics iST protein sample preparation for LC-MS kit (Preomics; Planegg/Martinsried, Germany) according to the manufacturer's instructions. The resulting purified peptides were resuspended in 30 µL nanoLC-Buffer A (5% acetonitrile, 0.2% formic acid). Samples were analyzed in protein profiling mode using an EASY-nLC 1200 liquid chromatography system (Thermo Fisher Scientific; Waltham, MA, USA) coupled to a Q-Exactive HF mass spectrometer (Thermo Fisher Scientific). Prior to mass spectrometry measurements, samples were diluted two-fold with nanoLC-Buffer A spiked with 1/10 iRT peptides (Biognosys; Schlieren, Switzerland); 2 µL of sample were injected and fractionated in a 50-cm-long C18RP RSLC ES803 Easyspray column (Thermo Fisher Scientific) at a flow rate of 200 nL/min with a 200-min gradient from nanoLC buffer A to 40% acetonitrile, 0.2% formic acid.

A *C. vulgaris* protein sequence database was derived from our own sequencing effort (Cecchin et al., 2019) and entries annotated based on species sequence orthology. Raw mass spectrometry data were processed using

the Spectronaut software package (Version 15, Biognosys) against the above-mentioned protein database in directDIA mode. A dataset containing potential protein contaminants and sequences of iRT peptides (Biognosys) used for retention time normalization was utilized for Spectronaut data processing. Further data processing was performed in the R statistical environment. For each protein, the obtained quantification values were summed for quantified peptides and charge states. Proteins with missing values in <50% of the samples were retained. Data were log-transformed and normalized for equal medians across all samples. For the detection of differentially expressed proteins, a linear model was fitted for the treatment, and control groups and p-values from moderated t-statistics were calculated with the empirical Bayes approach (Gentleman et al., 2004). The Benjamini-Hochberg False Discovery Rate (FDR) method was used to correct for multiple hypotheses testing.

Gene-set enrichment analysis (GSEA) was performed using the GSEA algorithm of the piano package for R (Väremo, Nielsen, & Nookaew, 2013). Log2 fold-changes were used as gene-level statistics and p-values were estimated by gene sampling, followed by fdr-adjustment for multiple hypothesis testing.

Gene Ontology (GO) terms related to identified proteins were visualized using REVIGO software (Supek, Bošnjak, Škunca, & Šmuc, 2011).

RESULTS

Pigment accumulation

C. vulgaris cells were acclimated to LL (70 µmol m^{-2} s^{-1}) or HL (850 µmol m^{-2} s^{-1}) growth conditions for at least 10 generations. We determined the light gradient experienced by the cell considering the pigment content and the transmittance of the culture at the different days (Fig. S1): the cells were exposed to a light gradient with the maximum range (bottom-top of the culture) of 70-25 µmol m^{-2} s^{-1} for LL cells and 800-310 µmol m^{-2} s^{-1} for HL cells. Cells grown in HL conditions were characterized by faster growth rate and increased biomass production compared to LL cells (Fig. S2). As reported in Table 1, cells grown in HL were characterized by a ~60% reduction in Chl content per cell. The residual Chl composition in HL samples was also changed compared to LL, with the Chl a/b ratio significantly increased at high irradiances. Carotenoid content was not significantly different on a cell basis but increased on a Chl basis in HL samples, with lutein representing ~70% of total carotenoids in both the LL and HL groups. In HL, zeaxanthin was also detectable, while the other xanthophylls (neoxanthin and violaxanthin) were significantly reduced on a cell basis in HL compared to LL. The reduced Chl b content and Chl/Car ratio in HL compared to LL suggest that exposure to different irradiances induced a reorganization of the photosynthetic apparatus.

Photosynthetic activity and mitochondrial respiration

The increased Chl a/b ratio in HL suggests a decrease of LHC antenna complexes per photosystem, since Chl b is only bound to external antenna subunits. Light-harvesting properties of PSII—also known as functional

"antenna size"—can be measured by following the Chl a fluorescence induction kinetic in DCMU-treated cells exposed to limiting light as fluorescence emission is inversely related to light-harvesting properties of PSII. As shown in Fig. 1A, HL cells were characterized by a slower fluorescence induction kinetic compared to LL cells, indicating a smaller antenna size (Table S1). In the case of PSI, its functional antenna size can be estimated by following the kinetics of P700 oxidation in limiting light in the presence of linear and cyclic electron transport inhibitors (DCMU and DBMIB) to fully inhibit P700 re-reduction, adding artificial electron donors and acceptors (ascorbate and methyl-viologen, respectively). As shown in Fig. 1B, there were no differences between HL and LL cells in the case of PSI antenna size.

LHCII antenna can migrate from PSII to PSI to balance the excitation pressure among the two photosystems in a process called state transitions (Finazzi et al., 2002; Lemeille, Turkina, Vener, & Rochaix, 2010; Nawrocki, Santabarbara, Mosebach, Wollman, & Rappaport, 2016). State transitions are triggered by the redox state of plastoquinones, with State 1 (S1) or State (S2) being the condition with minimum or maximum migration of LHCII to PSI, respectively; they can be induced by consuming (S1) or increasing (S2) the reducing power in the chloroplast (Fleischmann et al., 1999). When state transitions occur, the migration of LHCII to PSI increases its fluorescence emission, which consequently decreases the emission of PSII. S1 and S2 state were then estimated by measuring fluorescence emission at 77K, where both PSI and PSII emissions are detectable. As shown in Fig. 1, increased state transition capacity was measured for LL-acclimated cells. This could be related to the presence of mobile LHC antenna proteins that could be lost upon HL acclimation.

Photosynthetic linear electron transport was then investigated by measuring light-dependent oxygen evolution. As shown in Fig. 2A, on a Chl basis, HL-acclimated cells were characterized by a higher oxygen evolution rate at light intensities greater than 500 $\mu mol\ m^{-2}\ s^{-1}$, with an almost three-fold increase in the maximum oxygen evolution rate (Pmax, Table 2). Due to reduced Chl per cell content, on a cell basis HL cells were evolving less oxygen compared to LL cells at lower actinic lights, but a similar oxygen production was achieved at higher illumination range (Fig. S3). HL-acclimated cells were thus more efficient on a Chl basis in using the available light energy to strip electron from water molecules and transport them across the photosynthetic electron transport chain. The impact of cyclic electron transport compared to linear electron transport was then evaluated by measuring the ECS in the presence or absence of DCMU, which inhibits linear electron transport. ECS is directly related to thylakoid membrane polarization due to electron and proton transport; in the presence of DCMU the ECS signal is only related to cyclic electron transport. In the absence of DCMU, there were no significant differences comparing HL- to LL-acclimated cells (Fig. 2B). However, in the presence of DCMU, reduced ECS was evident in the case of LL-acclimated cells. The relative contribution of cyclic electron transport to the ECS signal is reported in Fig. 2C for HL- and LL-acclimated cells at the different actinic lights measured, being significantly higher for HL cells. The increased cyclic electron transport contribution to overall photosynthetic electron transport suggests an increased ATP/NADPH ratio in HL for the cofactors produced in the light phase of photosynthesis, as cyclic electron transport is only related to lumen acidification and ATP biosynthesis.

PSI and PSII photosynthetic activities were then measured in HL- compared to LL-acclimated cells. In the case of PSI, P700 photochemical activity on a Chl basis was higher in HL versus LL (Fig. 3A). PSII photosynthetic properties were then analyzed by measuring the fluorescence-based parameters Y(II), 1-qL, and NPQ (Fig. 3B-E), representing the PSII quantum yield, the redox state of plastoquinone, and the capacity to thermally dissipate of the light energy absorbed, respectively. Y(II) was higher for HL-acclimated cells for actinic lights up to 1400 µmol $m^{-2}s^{-1}$, indicating increased photochemical efficiency. Consistently, 1-qL values were lower in the same light range in HL cells, suggesting that the plastoquinone pool was less reduced and the photosynthetic electron transport chain less saturated.

The activity of PTOX in LL and HL cells was then investigated being correlated to plastoquinone oxidation by chlororespiration. PTOX activity can be measured following the PSII fluorescence kinetics upon light to dark transition in presence or absence of the PTOX inhibitor n-propylgallate (PG) (Houille-Vernes, Rappaport, Wollman, Alric, & Johnson, 2011). As shown in Fig. S4, in the case of LL cells, light to dark transition caused a fast decay of fluorescence emission, which was delayed in presence of PG. This result demonstrates that PTOX is active in LL cells and contributes to plastoquinones oxidation transferring electrons to oxygen. In the case of HL cells, a more complex situation was evident: without inhibitor, a transient dark rise of fluorescence was measured upon light to dark transition suggesting that when the light is turned off a transient plastoquinone pool reduction occurs due to the high reducing power in the chloroplast which cannot be consumed by carbon fixation pathway. In presence of PG, HL cells was characterized by a continuous rise of fluorescence upon light to dark transition, indicating an important effect of PTOX on relaxing plastoquinone pool which is essential in HL cells to properly balance the redox state of plastoquinones.

NPQ induction was characterized by complex kinetics: NPQ was induced to a higher level in HL-acclimated cells exposed to actinic light compared to the LL case, but after ~1 minute of light exposure, NPQ relaxed and reached values similar to LL cells. When actinic light was turned off, NPQ dark relaxation was reduced in LL cells compared to HL, demonstrating increased qE induction in HL, as qE is the fast-relaxing component of NPQ induced by lumen acidification. This behavior was observed for all the different actinic lights (Fig. S5). NPQ relaxation during actinic light exposure was suggested to be related to the activation of Calvin cycle enzymes that consume NADPH and ATP and restore their precursors $NADP^+$ and ADP, which are required to desaturate the photosynthetic electron transport chain (Cardol, De Paepe, Franck, Forti, & Finazzi, 2010).

NAD(P)H /NAD(P) balance was thus analyzed following fluorescence emission at ~500 nm, where the reduced NAD(P)H form emits, upon exposure to actinic light followed by dark relaxation. It is important to note that is not possible to discriminate between NADH and NADPH following 500-nm fluorescence emission, and the results obtained are related to the overall balance of NAD(P)H oxidation and reduction in the whole cell. As depicted in Fig. 3F, NAD(P)H fluorescence was initially increased upon exposure to actinic light in both LL and HL, indicating $NADP^+$ reduction; in the case of HL-acclimated cells, NADPH fluorescence emission reached a steady state, resulting from a similar rate of NADPH oxidation and $NADP^+$ reduction. In LL-acclimated cells, a continuous increase in NAD(P)H fluorescence was measured during actinic light

exposure, suggesting relatively faster $NAD(P)^+$ reduction than NADPH oxidation, with a consequent decrease in the amount of $NAD(P)^+$ available as acceptors for electrons transported across the photosynthetic electron transport chain. These results are indeed consistent with the increased PTOX activity, being able to prevent overreduction of chloroplast reducing power, and with the increased photosynthetic rates measured on a Chl basis in HL cells at the actinic light herein used for NAD(P)H measurement (Fig. 2A). When the light was turned off, the NAD(P)H fluorescence signals decreased in both LL- and HL-acclimated cells, but the signal slowly and partially recovers after few seconds, indicating ongoing $NAD(P)^+$ reduction that is likely related to light-independent NAD(P)H formation through the pentose phosphate pathway and/or by glycolysis and tricarboxylic acid (TCA) pathways.

Next, we evaluated mitochondrial respiration (Fig. 4) and found increased oxygen consumption rate in the dark in the case of HL-acclimated cells compared to LL. The contribution of cytochrome and alternative pathways was then investigated by measuring dark respiration in the presence of two specific inhibitor: SHAM that inhibits AOX and the alternative pathway, and myxothiazol that locks complex III, thereby blocking the cytochrome pathway (Dang et al., 2014). The sums of the estimated alternative and cytochrome respiratory pathways, even if slightly decreased, were not significantly different compared to the total dark respiration measured in absence of inhibitors. The increased mitochondrial respiration in HL-acclimated cells was due specifically to the increased alternative pathway activity (Fig. 4). Electron transport through AOX is not coupled with proton transport across the inner mitochondrial membrane, and it does not induce ATP biosynthesis. The relatively higher alternative pathway activity in HL-acclimated cells indicates more rapid regeneration of NAD^+. Higher AOX and PTOX activity in HL acclimated cells likely allow to properly tune the reducing power of chloroplast and mitochondria, preventing overreduction of electron transport carries, consistently with the case of the extremely high light tolerant strain *Chlorella ohadii* (Treves et al., 2020).

Proteomic analysis

To investigate the molecular details underlying acclimation to HL or LL conditions, we performed a comparative proteomic analysis on protein extracts from acclimated cells. Microalgal proteins were extracted, digested, and purified to obtain peptides, which were separated using reversed-phase nano liquid chromatography (nanoLC) and analyzed by an Orbitrap mass spectrometer (see Materials and Methods section for details). A direct data-independent acquisition (directDIA) method was leveraged to determine protein compositions and differential protein abundances under the two acclimation conditions. In total, 4457 proteins were identified and quantified (Dataset S1), demonstrating an improved resolution compared to previous proteomic datasets obtained from *C. vulgaris*, where less than 3000 proteins were identified (Guarnieri, Nag, Yang, & Pienkos, 2013). Protein content per cell was similar in HL and LL cells (Fig. S6A) but the protein percentage of dry weight was reduced in HL (Fig. S6B), consistently with previous finding (Cecchin et al., 2019). Differential protein expression was then analyzed (Fig. 5). It is important to note that even if the different replicates analyzed were characterized by a similar growth curve for each condition (Fig. S2), there

was more variance in HL cells compared to LL cells in terms of protein expression as reported by PCA analysis (Fig. 5A), suggesting a more dynamic adjustment of protein expression in the former: the higher growth rates of HL cells compared to LL ones imply a more transition between the different cell growth phases, possibly increasing the variance during samplings. The volcano plot obtained upon expression analysis demonstrates that most of the identified proteins were not differentially expressed in HL vs. LL conditions (Fig. 5B). Accordingly, considering adjusted p-values below 0.05, only 89 and 147 proteins resulted respectively as upregulated and downregulated in HL, with a log2 fold change >1 or <-1 (Dataset S2). The top 10 upregulated or downregulated proteins in HL vs. LL are shown in Fig. 4C. Gene-set enrichment analysis (GSEA) was then performed on the GO terms retrieved (Fig. 5C): significant results were obtained only for GO terms downregulated in HL, most of which involved in the light phase of photosynthesis as PSI and PSII components, Chl binding proteins and/or proteins located in the thylakoidal membranes. This result is consistent with the decrease in Chl content per cell observed in HL vs. LL cells (Table 1). Moreover, significant enrichment of proteins with peptidyl-prolyl isomerase activity were identified as downregulated in HL (Table S2): peptidyl-prolyl isomerases catalyze cis–trans isomerization of peptide bonds N-terminal to proline residues in polypeptide chains, a key step for protein folding. Significant enrichment of GO terms encoding for cytosolic large ribosomal subunits was also identified as downregulated in HL, suggesting a general decrease of protein biosynthesis in HL cells, consistently with the reduced percentage of protein content per dry weight at high irradiance. To provide a more general view of the protein expression in HL vs. LL conditions, GO terms resulting after GSEA with adjusted p-value below 0.25 were visualized by REVIGO tool (Supek et al., 2011) analyzing separately the enriched GO terms resulting as upregulated or downregulated in HL (Fig. S7). In addition to the main GO terms downregulated in HL, as those involved in photosynthesis and peptidyl-prolyl isomerases, REVIGO analysis allowed to identify "ATP binding" and "intracellular transport" as enriched GO terms upregulated in HL at the limit of significancy (adjusted p-value of 0.056). Moreover, the most significant enriched GO terms referred to cellular comportments were related to the mitochondria for upregulated genes and to the chloroplast envelope, plastoglobuli and photosystems for genes downregulated in HL vs. LL. The GO terms and Kegg Orthology identifiers of the differentially expressed proteins were then used to analyze their functions are described below and summarized in Fig. 6.

Photosynthesis

Cells acclimated to HL were characterized by downregulation of several proteins annotated as LHC subunits. In particular, most of the proteins previously annotated in *C. vulgaris* as antenna proteins of PSI (Lhca) or PSII (Lhcb) (Cecchin et al., 2019) were downregulated in HL-acclimated cells. Similarly, several subunits of the PSI and PSII core complexes were downregulated in HL (Table S3). These results are consistent with the reduced Chl content per cell measured in HL compared to LL (Table 1). The reduced accumulation of PSI, PSII and LHCII subunits was then confirmed by western blot analysis using α-PsaA (subunit of PSI core complex), α-CP43 (subunit of PSII core complex) and α-LHCII antibodies (Fig. S8). HL cells also showed downregulation of Low PSII Accumulation (LPA) protein expression. These proteins are involved in PSII

assembly, and gene deletions in *A. thaliana* or *C. reinhardtii* severely impaired PSII accumulation (Cecchin, Jeong, et al., 2021; Schneider et al., 2014; Spaniol et al., 2022; Wakao et al., 2021). Interestingly, no significant differential expression for proteins involved in carbon fixation was found in HL vs. LL *C. vulgaris* cells (Dataset S3). This result was confirmed on a cell basis by western blot analysis in the case of the large subunit of RUBISCO (Fig. S8). It is interesting to note that, being the Chl content per cell reduced in HL, the similar RUBISCO content per cell means an increased accumulation of the main enzyme involved in carbon fixation on a Chl basis in HL conditions: the increased RUBISCO content per Chl could contribute to the increased electron transport properties measured in the case of HL cells, due to increased regeneration of ATP and NADPH precursors. A protein predicted as chloroplast ferredoxin-thioredoxin reductase (g1978.t1) was downregulated in HL. This enzyme is involved in activation of Calvin cycle enzyme depending on the redox state of the chloroplast. The plastid localization of the g1978.t1 gene product was confirmed by TargetP, and its downregulation in HL indicates that catalysis of thioredoxin-based activation of the Calvin cycle enzyme is more required in LL rather than HL conditions. Finally, HL cells were characterized by reduced accumulation of proteins encoded by g10107.t1 and g5581.t1 genes, predicted as carbonic anhydrase, a component of the CCM (Carbon-Concentrating Mechanism). The CCM is found in microalgae and enables an increased intracellular concentration of CO_2 (Wang, Stessman, & Spalding, 2015; Yamano, Miura, & Fukuzawa, 2008). It is possible that the increased carbon flow and mitochondrial respiration in HL conditions enhance CO_2 concentrations in the cells, which would induce a decrease in CCM activity (Fig. 6).

Pigment biosynthesis

Coproporphyrinogen III oxidase (g5001.t1), chlorophyll(ide) b reductase (g9809.t1), and porphobilinogen deaminase (g4163.t1) are enzymes involved in Chl biosynthesis and were reduced in HL-acclimated cells. This observation is consistent with the reduced Chl content per cell observed for HL compared to LL. In the case of carotenoid biosynthesis, the only enzyme identified as significantly differentially expressed was zeaxanthin epoxidase (g9297.t1), which was downregulated in HL, while the violaxanthin de-epoxidase enzyme was downregulated in HL at the limit of the threshold herein considered (p-value of 0.05 and log2 fold change >1, Dataset S3). Both zeaxanthin epoxidase (ZE) and violaxanthin de-epoxidase (VDE) are involved in the zeaxanthin metabolism: ZE catalyzes the epoxidation of zeaxanthin to antheraxanthin and violaxanthin, while VDE is the enzyme that upon light stress triggers the conversion of violaxanthin into zeaxanthin. The decreased expression of ZE in HL cells is in line with the increased zeaxanthin fraction of total carotenoids measured in HL-acclimated cells (Table 1). Similarly, the reduced violaxanthin content in HL reduces the requirement of VDE enzyme, being a significant fraction of zeaxanthin already accumulated. It is important to note that zeaxanthin is involved in several photoprotective mechanisms in *C. vulgaris* (Girolomoni et al., 2020).

Nitrogen assimilation and amino acid metabolism

Ferredoxin nitrate reductase (g9255.t1) was downregulated in HL-acclimated cells. Nitrate reductases are chloroplast enzymes required for nitrogen assimilation to produce ammonia from nitrate, which was provided to LL and HL cells as nitrogen source during growth. Considering the requirement of ammonia for Chl

biosynthesis, nitrate reductase expression is likely linked with the regulation of pigments accumulation at different growth irradiances. Accordingly, ferredoxin nitrate reductase expression was reduced in HL conditions, as was the Chl content per cell. Considering the increased growth rate observed for cells grown in HL, we cannot exclude that nitrogen assimilation fluxes could be similar or even increased in HL vs. LL cells due to post translational regulation. Several enzymes involved in amino acid catabolic metabolism were upregulated in HL-acclimated cells, including 2-oxoisovalerate dehydrogenase E1 component alpha subunit (g10682.t1) and 3-methylcrotonyl-CoA carboxylase alpha subunit (g10016.t1) involved in leucine degradation, with the former also catalyzing reactions involved in valine and isoleucine degradation. In HL-acclimated cells, enzymes catalyzing transfer or removal of nitrogenous groups were also upregulated, such as L-asparaginase (g5102.t1) and aromatic amino acid aminotransferase II (g7030.t1). Moreover, increased accumulation of three proteases was observed in HL (g8295.t1, g1394.t1, and g10206.t1): upregulation of enzymes involved in amino acid degradation could be related to a strategy to recycle the amino group when nitrate reductase expression is decreased. Increased amino group recycling could also be related to increased photooxidative stress in HL cells and increased protein damage.

Sulfur assimilation

Sulfur assimilation requires sulfate import into cells, which is activated by adenylation of adenosine 5′-phosphosulfate (APS). APS can then be reduced to produce sulfite, which can be used for cysteine and methionine biosynthesis, or phosphorylated to produce PAPS (3′-phosphoadenosine-5′-phosphosulfate), which serves as a sulfate donor to synthesize sulfated metabolites (Klein & Papenbrock, 2004). In the case of the sulfur assimilation pathway, the enzyme adenylyl-sulfate kinase (g1541.t1) that catalyzes APS phosphorylation was downregulated in HL. Downregulation of enzymes involved in APS phosphorylation was previously observed in *A. thaliana* in the setting of sulfur deficiency, when sulfate transporters are upregulated (Bohrer, Kopriva, & Takahashi, 2014). Consistently, a sulfate transporter (g7389.t1) was upregulated in HL-acclimated cells, while a predicted homocysteine S-methyltransferase (g5360.t1) involved in methionine biosynthesis was downregulated in HL. Moreover, upregulation of adenylyl-transferase and sulfotransferase MOCS3-like protein (g360.t1) was observed in HL cells; this enzyme is involved in molybdenum cofactor biosynthesis and thiocarboxylation of the adenylated C-terminal glycine of the ubiquitin-related modifier 1 (URM1) (Mayr, Mendel, & Schwarz, 2021). URM1 is either involved in thiolation of tRNA or urmylation of target proteins (Nakai, Harada, Hashiguchi, Nakai, & Hayashi, 2012; Schmitz et al., 2008). Urmylation is a post-translation protein modification that is reportedly involved in oxidative stress in plants and nutrient sensing and budding in yeast (Goehring, Rivers, & Sprague, 2003). The role of urmylation in microalgae has not been sufficiently investigated, but in *C. vulgaris* a homolog of URM1 is encoded by gene g314.t1 (Fig. S10), which was not differentially expressed in HL vs. LL conditions.

Nucleotide metabolism

HL-acclimated cells were characterized by upregulation of a predicted ribonucleoside-diphosphate reductase (g6171.t1). This key enzyme for purine and pyrimidine metabolism catalyzes the formation of deoxyribonucleotides from ribonucleotides. Increased nucleotide biosynthesis could be related to the higher growth rate observed in HL-acclimated cells (Cecchin et al., 2019), as more DNA replication is required for cell division.

Intracellular transport and trafficking

Several proteins involved in intracellular transport and trafficking were upregulated in HL (Table S4), including a Sec24-like subunit involved in vesicle formation. Moreover, several intracellular and extracellular transport components were upregulated in HL, including transporters for amino acids (g8327.t1, g1827.t1, g1828.t1, and g9008.t1). Differently, HL cells showed downregulation of a peptide ABC transporter (g6888.t1). These findings suggest a reorganization of amino acid and peptide transport in cells upon acclimation to different light intensities. It is interesting to note that in HL cells a protein annotated as being in the MATE (Multidrug And Toxic Compound Extrusion) efflux family (g9504.t1) was strongly upregulated. The MATE protein family was reported to be involved in detoxification processes in different organisms, including land plants and microalgae (Nimmy et al., 2022). The increased accumulation of a MATE protein in HL cells suggests a role of this subunit for HL acclimation.

Lipid metabolism

Enzymes involved in lipid biosynthesis or catabolism were generally not differentially expressed in HL- vs. LL-acclimated cells, with the exception of downregulation of a caleosin/peroxygenase 2-like protein (g8244.t1) in HL (Dataset S3). This protein is a predicted calcium-binding peroxygenase involved in the degradation of oil bodies (Rahman et al., 2018), and its downregulation in HL is consistent with the increased lipid and triacylglycerol accumulation in HL cells previously reported for *C. vulgaris* (Cecchin et al., 2019). A solanesyl diphosphate synthase (g5152.t1) was also upregulated in HL. Solanesyl diphosphate synthase is an enzyme involved in ubiquinone and plastoquinone biosynthesis, where plastoquinones are required to desaturate the photosynthetic electron transport chain. Previous work demonstrated dual localization of solanesyl diphosphate synthase in the chloroplasts and mitochondria of plants (Ohara, Sasaki, & Yazaki, 2010). In the case of the g5152.t1 gene product, it was not possible to identify a transit peptide for chloroplasts or mitochondria, and further work is required to investigate the localization of function for this enzyme. Finally, enzymes involved in sterol biosynthesis were upregulated in HL, including an NADPH:adrenodoxin reductase (g1319.t1), a cytochrome P450 (g7370.t1), and a 3-beta-hydroxysteroid-Δ8, Δ7-isomerase (g6761.t1). Steroid metabolites (ergosterol and brassicasterol) were previously shown to be produced in *Chlorella* species, and sterol content was reportedly enhanced at increasing irradiances in various microalgal species (Randhir, Laird, Maker, Trengove, & Moheimani, 2020).

Mitochondrial oxidation pathways

A mitochondrial succinate dehydrogenase assembly factor (g8306.t1) was upregulated in HL cells. Succinate dehydrogenase is an enzyme involved in the TCA cycle that strips electrons from succinate and reduces ubiquinone to fuel oxidative phosphorylation reactions. Increased accumulation of mitochondrial succinate dehydrogenase assembly factor is thus consistent with the higher level of mitochondrial respiration observed in HL. It is important to note that one of the proteins with the strongest upregulation in HL-acclimated cells was a phosphate acetyltransferase (PAT encoded by g6335.t1). This enzyme catalyzes the reversible production of acetate from acetyl phosphate, which can be produced by acetyl-CoA synthase (ACS). The gene product of g6335.t1 has a predicted mitochondrial target peptide; in *C. reinhardtii*, ACS and PAT enzymes were identified both in the mitochondria and plastids, where they are involved in dark fermentation of sugars to produce acetate (Yang et al., 2014). It is possible that the increased carbon flow in HL-acclimated cells enhances the production of acetyl-CoA, which can be converted into acetate that then diffuses back to the chloroplast or the cytosol as a precursor for fatty acid biosynthesis (Cecchin et al., 2019; Lin & Oliver, 2008). Interestingly, HL-acclimated cells exhibited increased accumulation of a protein annotated as adenylate kinase (g3460.t1). Its localization is predicted in the mitochondria, while other two adenylate kinases located in chloroplasts (g1121.t1, g2609.t1) were downregulated in the same growth conditions. Adenylate kinase enzymes are involved in the regulation of ATP, ADP, and AMP homeostasis; they catalyze the reversible reaction where a phosphate group is transferred from ATP to AMP to form two ADP molecules (Lange, Geserick, Tischendorf, & Zrenner, 2008). The reduced accumulation of adenylate kinase in chloroplasts in HL-acclimated cells can be explained by the increased requirement of ATP for CO_2 assimilation at high irradiances and the consequent continuous regeneration of ADP. Differently, the greater accumulation of mitochondrial adenylate kinase in HL cells could be related to increased carbon flow and mitochondrial respiration which require higher ADP availability for ATP production and relaxation of the proton gradient across the inner mitochondrial membrane generated by NADH oxidation.

Signaling and gene expression

It is interesting to note that the protein with the highest fold changed in HL compared to LL (g7323.t1, Fig. 5C) was found to have 71% and 80.7% of identity and similarity, respectively, with a heliorhodopsin previously identified in *Chlorella variabilis* (Pushkarev et al., 2018) (Fig. S9). Heliorhodopsins are microbial-like rhodopsins previously suggested to have light-sensing activity (Chazan et al., 2022; Kovalev et al., 2020), which could be required for adaptation of *C. vulgaris* cells to grow under high irradiance. In HL, other signaling proteins were identified among the top-10 upregulated proteins, such as the Gpr1-like protein (g8989.t1; g8994.t1). Gpr1 is a member of the G protein-coupled receptor family and is likely a component of the signaling pathway underlying the physiologic response triggered by HL acclimation. Notably, a protein annotated as TBC1 domain family member 2A (g4132.t1) was also upregulated in HL. Proteins with TBC domains have been reported in different organisms from humans to plants as GTP-ase activating subunits that deactivate the signaling function of G proteins (Pan, Eathiraj, Munson, & Lambright, 2006), likely acting as a specific component of signaling pathways for cell acclimation in HL. Moreover, a subunit (subunit 6) of the

COP9 signalosome (g8205.t1) was upregulated in HL-acclimated cells. COP9 is a protein complex initially characterized in plants but then found in several eukaryotic organism; it is involved in the activation of E3-cullin RING ubiquitin ligases (CRLs) that further control protein degradation through ubiquitination (Barth, Hübler, Baniahmad, & Marz, 2016). In plants, COP9 is a component of photoreceptor-mediated signaling (Chamovitz et al., 1996; Wei, Chamovitz, & Deng, 1994), and its increased accumulation in HL suggests a specific role in cell responses at higher irradiances, even if the role of COP9 in microalgae has not been fully elucidated. Several kinases and phosphatases were upregulated in HL, while only a histidine kinase (g6989.t1) and a LRR (leucin-rich repeat) receptor-like serine/threonine kinase (g5516.t1) were reduced in HL compared to LL-acclimated cells (Table S5). LRR receptor-like serine threonine- kinases belong to a multigene family considered to be the largest family of plant receptor kinases that is reportedly involved in plant development and immunity (Afzal, Wood, & Lightfoot, 2008; De Smet, Voss, Jürgens, & Beeckman, 2009), but their relevance in microalgae remains unclear. Interestingly, three different gene products annotated as chloroplast aarF domain-containing kinase (g5742.t1, g9784.t1, and g7165.t1) were upregulated in HL cells. The protein homolog of aarF domain-containing kinase in *Arabidopsis thaliana* was renamed ABC1K1 (activity of bc1 complex kinase 1) and was associated to plastoglobuli with a role in triggering the biosynthesis of plastoquinone and carotenoid that are required to prevent or mitigate photo-oxidative stress (Martinis et al., 2014). For this reason, ABC1K1 activity can be linked with HL acclimation mechanisms in *C. vulgaris* cells, which are more likely to experience photo-oxidative stress than cells grown in LL.

Transcription factors are usually low abundant compared to other proteins and their identification by proteomic analysis is not trivial (Simicevic & Deplancke, 2017; Simicevic et al., 2013): here 83 different putative transcription factors were identified (Dataset S3). Only two putative transcription factors were differentially expressed in HL vs. LL cells. The products of genes g5610.t1 and g2204.t1 were both annotated as transcription factors and upregulated and downregulated in HL, respectively. It is interesting to note HL upregulation of proteins predicted as HASTY1 (g1408.t1) and TRANSPORTIN1 (g10026.t1). Their homologous proteins in *A. thaliana* were reported to have a function in miRNA activity; HASTY1 favors the nuclear export of miRNA, while TRANSPORTIN1 mediates the interaction between miRNA and ARGONAUTE, a protein required for miRNA-mediated post-transcriptional regulation.

DISCUSSION

Acclimation to the different growth conditions is a key parameter to be considered for microalgae cultivation in artificial systems. Different cultivation set-ups imply varied exposure of cells to light, CO_2, nutrients, and temperature, which may significantly influence the biomass and biomolecular properties of the cultivated strains. In the case of *C. vulgaris*, our results reveal a different situation compared to the model organism for green algae *C. reinhardtii.* Indeed, *C. reinhardtii* acclimation to HL does not influence the stoichiometry of antenna subunits per PSII, but it is accompanied by a strong increase in its photoprotective properties, with increased capability of NPQ induction (Bonente et al., 2012). In *C. vulgaris*, HL acclimation was associated

with reduced accumulation of both LHC and the core subunits of PSI and PSII, with a reduced functional antenna size in the case of PSII, similar to the case of land plants acclimated to high irradiances (Ballottari, Dall'Osto, Morosinotto, & Bassi, 2007). *C. vulgaris* HL-acclimated cells were also characterized by different NPQ dynamics compared to LL cells. Even if the total NPQ observed at the end of light exposure was similar in HL- and LL-acclimated cells, the former induced a higher qE (the fastest component of NPQ), and cells showed higher NPQ values during the first minute of illumination. The key proteins involved in qE, such as LHCSR (light harvesting complex stress related) and PSBS subunits, were not differentially accumulated in HL vs. LL cells; however, considering the reduced PSII core observed in HL, higher PSBS/PSII and LHCSR/PSII contents are consistent with the observations of different NPQ dynamics and increased qE.

The reduced accumulation of Chl binding proteins in *C. vulgaris* cells grown in HL is consistent with previous findings in the case of *C. reinhardtii* or *Synechocystis sp. PCC 6803* (Toyoshima et al., 2019). Moreover, a conserved features between *C. reinhardtii, Synechocystis sp. PCC 6803* and *C. vulgaris* acclimation to HL is the unchanged accumulation of carbon fixing enzymes on a protein basis, but while ATP synthase and NDH subunits were upregulated in HL in *Synechocystis sp. PCC 6803*, this was not the case for *C. reinhardtii* (Toyoshima et al., 2019) or *C. vulgaris* (this work), suggesting a peculiar adaptation in cyanobacteria, where photosynthetic electron transport and respiration shares several electron carriers and ATP biosynthetic enzymes. For both *C. reinhardtii* and *C. vulgaris*, HL acclimation resulted in improved photosynthetic activity with increased PSI activity, reduced saturation of the photosynthetic electron transport chain, and improved light-dependent oxygen evolution. The adaption observed for the photosynthetic electron transport chain allows cells to properly use the higher availability of photons in HL, increasing the excitation pressure on PSI—which has a higher photochemical efficiency compared to PSII—and allows them to rapidly oxidize plastocyanin and consequently plastoquinones, the electron acceptors for PSII. Moreover, the contribution of PTOX in oxidizing plastoquinones was higher in HL cells, revealing chlororespiration as a strategy to desaturate the photosynthetic electron transport as previously reported in the case of the light tolerant *Chlorella ohadii* (Kedem et al., 2021). The increased solanesyl diphosphate synthase content suggests a key requirement for HL cells to have sufficient plastoquinone and ubiquinone availability as electron carriers. The consequences of these adaptations are evident from the light dependent oxygen evolution curves of HL grown cells, having an increased efficiency on a Chl basis of PSII in stripping electrons for water, releasing oxygen, and fueling the photosynthetic electron chain. It is interesting to note that a relative increase in cyclic electron transport could also be measured in HL-acclimated cells from ECS measurements, leading to a potential increase of the ATP/NADPH ratio for the ATP and NADPH produced in the light phase of photosynthesis. Despite the higher photosynthetic electron flow in HL cells, the ECS signals were similar in HL vs. LL cells, demonstrating that increased proton pumping in the lumen—associated with increased electron transport—was rapidly used to produce ATP rather than induce lumen acidification.

HL cells grew faster and reached a higher biomass concentration compared to *C. vulgaris* grown in LL. Increased biomass production in HL cells requires more CO_2 fixation, which is consistent with the increased

photochemical activity leading to greater ATP and NADPH production (Fig. 6). Moreover, the content of RUBISCO was increased in HL cells on a Chl basis (Fig. S8), suggesting an increased capacity of carbon fixation enzymes to consume the products of photosynthetic light phase. ATP consumption by CO_2 fixation reactions release its precursor ADP, which can be used by thylakoidal ATP synthase, leading to efficient proton flux back to the stroma. Similarly, light-dependent NADPH consumption implies rapid regeneration of $NADP^+$ as an electron acceptor for photosynthetic electron transport. Consequently, upon light exposure $NAD(P)H/NAD(P)^+$ quickly reaches a balanced pseudo-stationary phase only in HL cells, whereas the reduction of NADPH exceeds its oxidation in LL cells (Fig. 2), leading to reduced $NADP^+$ availability and increased risk of saturation of the photosynthetic electron transport chain.

Increased carbon fixation leads to greater carbon flow through the cell with effects on metabolism (Fig. 6); mitochondrial activity was indeed affected by the light used for growth, with increased mitochondrial respiration observed in HL cells. According to the results obtained with specific inhibitors of the mitochondrial electron transport chain, the increased respiration in HL cells was mainly due to higher activity in the alternative electron transport pathway, which does not produce ATP but consumes reducing power. We can speculate that in HL cells, the higher carbon flow toward the mitochondria driven by increased carbon fixation induced an increased electron flow toward NADH or ubiquinones that must be oxidized to prevent unbalanced availability of oxidized cofactors. Accordingly, the proteomic analysis revealed that a succinate dehydrogenase enzyme involved in the TCA that causes reduction of ubiquinone was upregulated in HL cells. The increased accumulation of an adenylate kinase predicted to be localized in the mitochondria suggests that a fraction of the ATP produced by the TCA cycle and oxidative phosphorylation is hydrolyzed to regenerate ADP. This is a different situation compared to the plastid, where excess ATP produced is rapidly consumed by carbon fixation reactions to regenerate ADP.

One of the adaptation mechanisms observed for acclimation to different light intensities observed in *C. vulgaris* shared with *C. reinhardtii* is the decrease in Chl content in HL cells (Table 1). Chl biosynthesis is strictly dependent on nitrogen assimilation; HL cells were characterized by reduced nitrate reductase expression with consequently reduced potential for nitrogen assimilation. However, both nitrogen assimilation and ammonium production are required for amino acid biosynthesis. HL cells were indeed characterized by upregulation of enzymes involved in the degradation of amino acids and amino acid transporters, suggesting amino acid catabolism as a strategy to recycle the amino groups in conditions where nitrogen assimilation is reduced to inhibit Chl biosynthesis. It is interesting to note that among the enzymes involved in amino acid catabolism that were upregulated in HL, we identified L-asparaginase, an enzyme for used as a treatment for acute lymphoblastic leukemia. *C. vulgaris* was suggested as a potential source of L-asparaginase (Ebrahiminezhad, Rasoul-Amini, Ghoshoon, & Ghasemi, 2014); here we showed that HL acclimation increased production of this enzyme.

HL acclimation was previously demonstrated in *C. vulgaris* to increase the lipid fraction of dry weight (Cecchin et al., 2019). In line with this, our proteomic analysis revealed that HL cells had lower expression of

a caleosin/peroxygenase 2-like protein, an enzyme involved in oil body degradation. No enzymes involved in lipid biosynthesis were upregulated in HL except for those involved in sterol biosynthesis. Increased sterol content was reported in different microalgae species exposed to high light (Randhir et al., 2020). The specific role of sterols in microalgae has not been sufficiently investigated, but these molecules are reportedly involved in membrane fluidity, membrane-associated metabolic processes, and signal transduction. Understanding the possible increase in sterol biosynthesis in HL cells and its importance for HL acclimation requires further dedicated work. Considering the possible market opportunity for sterols produced by microalgae (Randhir et al., 2020), the evaluation of the influence of irradiance of growth on the sterols production yield could pave the way for specific biotechnological applications.

Acclimation to different irradiances implies the activation of cell signaling mechanisms controlling the activities of specific proteins and gene expression. Only two transcription factors were differentially expressed in HL vs. LL cells of *C. vulgaris*. Identifying transcription factors by proteomic analysis is challenging due to their low abundance in protein extracts. However, the identification of g2204.t1 and g5610.t1 gene products upregulated in LL and HL, respectively, suggest their major role controlling the gene expression patterns at these irradiances. A member of the heliorhodopsin protein family had one of the highest fold changes in HL, suggesting that photoreceptors may be involved in triggering cell adaptations to increased irradiances (Fig. 6). Moreover, subunit 6 of the COP9 signalosome was upregulated in HL, and COP9 is a component of photoreceptor-mediated signaling in plants exposed to HL (Chamovitz et al., 1996; Wei et al., 1994). Other possible components of this signaling mechanism include a Gpr1-like protein, a GTP-ase activating subunit (TBC domain-containing protein), and several kinases and phosphatases (Table S4). It is intriguing that the aarF domain-containing kinases (g5742.t1, g9784.t1, and g7165.t1) were upregulated in HL cells, since their homolog in *A. thaliana* (ABC1K1) was reported to be associated with plastoglobuli-triggering plastoquinone and carotenoid biosynthesis (Martinis et al., 2014).

In conclusion, we clarified some specific mechanisms activated in *C. vulgaris* cells following long-term exposure to LL or HL. Photosynthetic activity was improved in HL conditions despite reductions in pigment content and light-harvesting properties. The increased energy availability in HL stimulates the photosynthetic apparatus to increase PTOX and PSI activity, allowing for more efficient desaturation of the photosynthetic electron transport chain. This, combined with increased carbon fixation and ADP and $NADP^+$ regeneration enables cells to prevent saturation of the photosynthetic apparatus. The possible increase in carbon flow in HL cells is likely at the base of the enhanced mitochondrial respiration in this condition, mainly related to increased alternative oxidative pathway activity without ATP production. The ATP demand in HL conditions is likely sufficiently supplied by photosynthetic activity in the chloroplasts. The proteomic analysis results clarified which proteins are differentially expressed in LL vs. HL, and the list included several enzymes involved in cell metabolism and intracellular transport. Moreover, several putative components of cell acclimation mechanisms were identified as differentially expressed, suggesting a major role for a heliorhodopsin homolog for cell response to different irradiances. It is worth to note that the increased AOX and PTOX activity in HL

cells and the capacity to prevent overreduction of $NAD(P)^+$ to NAD(P)H is a shared feature between HL acclimated C. vulgaris and the extremely high light tolerant *C. ohadii,* where this adaptations were even more evident (Treves et al., 2020): the capacity to properly tune the redox state of mitochondria and chloroplast is likely a key strategy to ensure survival and high growth rate in HL conditions. The results described here suggest that a specific mutagenesis approach is required to elucidate the specific functions of the different proteins identified and clarify their possible roles in acclimation to different irradiances.

SUPPLEMENTARY DATA

Dataset S1. Proteins identified by proteomic analysis of Chlorella vulgaris cells grown in high light (HL) or low light (LL) conditions.

Dataset S2. Differentially expressed proteins in high light (HL) vs. low light (LL) acclimated *Chlorella vulgaris* cells.

Dataset S3. List of proteins identified by proteomic analysis involved in different metabolic pathways.

Table S1. PSII antenna size of *Chlorella vulgaris* cells acclimated to LL or HL.

Table S2. Differently expressed proteins annotated as peptidylprolyl isomerase.

Table S3. Differently expressed proteins involved in the light phase of photosynthesis.

Table S4. Differently expressed proteins in HL vs. LL involved in transport and trafficking.

Table S5. Differently expressed proteins in HL vs. LL involved in cell signaling.

Fig. S1: Transmittance of the cell cultures and estimation of light gradient in LL and HL conditions.

Fig. S2: Growth curves, growth rates and dry weight of *Chlorella vulgaris* cells in LL and HL conditions.

Fig. S3: Light curves of LL- and HL-acclimated cells measured as net light-dependent oxygen evolution. rates at different actinic lights normalized on a cell basis.

Fig. S4: PTOX activity in HL and LL acclimated *Chlorella vulgaris* cells.

Fig. S5: NPQ kinetics at different actinic lights.

Fig. S6: Protein content per cell and per dry weight in LL and HL conditions.

Fig. S7: REVIGO software visualization of all GO terms resulting upon Gene Set Enrichment Analysis (GSEA).

Fig. S8: Western blot analysis of photosynthetic proteins

Fig. S9. Alignment of g7323.t1 gene product with heliorhodopsin proteins.

699 Fig. S10. Alignment of g314.t1 gene product with URM1 protein encoded in the human genome.

700

701 **AUTHOR CONTRIBUTIONS**

702 MB: conceptualization; MC, JS, LC, MH, LG, SC: investigation; JS, MH: data curation; JS, MH, JH, NI, BT:
703 methodology; MB, CR, NI, BT: supervision; MC, SC, JS: visualization; MB: writing - original draft; MB, JS,
704 MC, SC, CR, NI, BT: writing - review & editing; MB, CR: funding acquisition

705

706 **ACKNOWLEDGMENTS**

707 We would like to thank Yvan Eb-Levadoux and Catherine Nury for computational assistance and establishing
708 the DIA proteomics workflow.

709 **CONFLICT OF INTEREST**

710 J.S., L.C., M.H., J.H., N.V.I., and B.T. are employees of Philip Morris International.

711

712 **FUNDING**

713 Philip Morris International funded the proteomics investigations. The research was supported by the ERC
714 Starting Grant SOLENALGAE (679814) to M.B. C.R. acknowledges FNRS-FWO EOS Project 30829584,
715 FNRS CDR J.0175.20, and Action de Recherche Concertée from the University of Liege (DARKMET ARC
716 grant 17/21–08).

717

718 **DATA SHARING AND DATA AVAILABILITY**

719 The mass spectrometry proteomics data have been deposited to the ProteomeXchange Consortium via the
720 PRIDE (Perez-Riverol et al., 2022) partner repository with the dataset identifier PXD037846.

REFERENCES

Afzal, A. J., Wood, A. J., & Lightfoot, D. A. (2008). Plant receptor-like serine threonine kinases: roles in signaling and plant defense. *Mol Plant Microbe Interact, 21*(5), 507-517. doi:10.1094/MPMI-21-5-0507

Allen, M. M., & Stanier, R. Y. (1968). Growth and division of some unicellular blue-green algae. *J Gen Microbiol, 51*(2), 199-202. doi:10.1099/00221287-51-2-199

Allorent, G., Tokutsu, R., Roach, T., Peers, G., Cardol, P., Girard-Bascou, J., . . . Finazzi, G. (2013). A dual strategy to cope with high light in Chlamydomonas reinhardtii. *Plant Cell, 25*(2), 545-557. doi:10.1105/tpc.112.108274

Ananyev, G., Gates, C., Kaplan, A., & Dismukes, G. C. (2017). Photosystem II-cyclic electron flow powers exceptional photoprotection and record growth in the microalga Chlorella ohadii. *Biochim Biophys Acta Bioenerg, 1858*(11), 873-883. doi:10.1016/j.bbabio.2017.07.001

Arnon, D. I., Tsujimoto, H. Y., & Tang, G. M. S. (1981). Proton transport in photooxidation of water: A new perspective on photosynthesis. *Proceedings of the National Academy of Sciences, 78*(5), 2942-2946.

Arriola, M., Velmurugan, N., Zhang, Y., Plunkett, M., Hondzo, H., & Barney, B. (2018). Genome sequences of Chlorella sorokiniana UTEX 1602 and Micractinium conductrix SAG 241.80: implications to maltose excretion by a green alga. *Plant Journal, 93*(3), 566-586. doi:10.1111/tpj.13789

Bailleul, B., Berne, N., Murik, O., Petroutsos, D., Prihoda, J., Tanaka, A., . . . Finazzi, G. (2015). Energetic coupling between plastids and mitochondria drives CO2 assimilation in diatoms. *Nature, 524*(7565), 366-+. doi:10.1038/nature14599

Baker, N. R. (2008). Chlorophyll fluorescence: a probe of photosynthesis in vivo. *Annu.Rev.Plant Biol., 59*, 89-113.

Ballottari, M., Dall'Osto, L., Morosinotto, T., & Bassi, R. (2007). Contrasting behavior of higher plant photosystem I and II antenna systems during acclimation. *J Biol Chem, 282*(12), 8947-8958. doi:10.1074/jbc.M606417200

Barth, E., Hübler, R., Baniahmad, A., & Marz, M. (2016). The Evolution of COP9 Signalosome in Unicellular and Multicellular Organisms. G*enome Biol Evol, 8(*4), 1279-1289. doi:10.1093/gbe/evw073

Bennoun, P. (1982). Evidence for a respiratory chain in the chloroplast. P*roceedings of the National Academy of Sciences, 79(*14), 4352-4356.

Bernaerts, T., Gheysen, L., Foubert, I., Hendrickx, M., & Van Loey, A. (2019). The potential of microalgae and their biopolymers as structuring ingredients in food: A review. B*iotechnology Advances, 37(*8). doi:10.1016/j.biotechadv.2019.107419

Blanc, G., Duncan, G., Agarkova, I., Borodovsky, M., Gurnon, J., Kuo, A., . . . Van Etten, J. L. (2010). The Chlorella variabilis NC64A genome reveals adaptation to photosymbiosis, coevolution with viruses, and cryptic sex. P*lant Cell, 22(*9), 2943-2955. doi:10.1105/tpc.110.076406

Boekema, E., & Braun, H. (2007). Supramolecular structure of the mitochondrial oxidative phosphorylation system. J*ournal of Biological Chemistry, 282(1*), 1-4. doi:10.1074/jbc.R600031200

Bohrer, A. S., Kopriva, S., & Takahashi, H. (2014). Plastid-cytosol partitioning and integration of metabolic pathways for APS/PAPS biosynthesis in Arabidopsis thaliana. Fr*ont Plant Sci, 5,* 751. doi:10.3389/fpls.2014.00751

Bonente, G., Ballottari, M., Truong, T. B., Morosinotto, T., Ahn, T. K., Fleming, G. R., . . . Bassi, R. (2011). Analysis of LhcSR3, a Protein Essential for Feedback De-Excitation in the Green Alga Chlamydomonas reinhardtii. Pl*os Biology, 9(1*). doi:10.1371/journal.pbio.1000577

Bonente, G., Pippa, S., Castellano, S., Bassi, R., & Ballottari, M. (2012). Acclimation of Chlamydomonas reinhardtii to Different Growth Irradiances. Jo*urnal of Biological Chemistry, 287(8*). doi:10.1074/jbc.M111.304279

Burlacot, A., Peltier, G., & Li-Beisson, Y. (2019). Subcellular Energetics and Carbon Storage in Chlamydomonas. C*ells, 8(1*0). doi:10.3390/cells8101154

Camacho, F., Macedo, A., & Malcata, F. (2019). Potential Industrial Applications and Commercialization of Microalgae in the Functional Food and Feed Industries: A Short Review. Ma*rine Drugs, 17(6*). doi:10.3390/md17060312

Cardol, P., De Paepe, R., Franck, F., Forti, G., & Finazzi, G. (2010). The onset of NPQ and Deltamu(H)+ upon illumination of tobacco plants studied through the influence of mitochondrial electron transport. Bi*ochim Biophys Acta, 1797(2*), 177-188. doi:10.1016/j.bbabio.2009.10.002

Cecchin, M., Jeong, J., Son, W., Kim, M., Park, S., Zuliani, L., . . . Jin, E. (2021). LPA2 protein is involved in photosystem II assembly in Chlamydomonas reinhardtii. Pla*nt Journal, 107(6)*, 1648-1662. doi:10.1111/tpj.15405

Cecchin, M., Marcolungo, L., Rossato, M., Girolomoni, L., Cosentino, E., Cuine, S., . . . Ballottari, M. (2019). Chlorella vulgaris genome assembly and annotation reveals the molecular basis for metabolic acclimation to high light conditions. Pla*nt Journal, 100(6)*, 1289-1305. doi:10.1111/tpj.14508

Cecchin, M., Paloschi, M., Busnardo, G., Cazzaniga, S., Cuine, S., Li-Beisson, Y., . . . Ballottari, M. (2021). CO2 supply modulates lipid remodelling, photosynthetic and respiratory activities in Chlorella species. Pla*nt Cell and Environment. d*oi:10.1111/pce.14074

Chamovitz, D. A., Wei, N., Osterlund, M. T., von Arnim, A. G., Staub, J. M., Matsui, M., & Deng, X. W. (1996). The COP9 complex, a novel multisubunit nuclear regulator involved in light control of a plant developmental switch. Cel*l, 86(1)*, 115-121. doi:10.1016/s0092-8674(00)80082-3

Chazan, A., Rozenberg, A., Mannen, K., Nagata, T., Tahan, R., Yaish, S., . . . Pushkarev, A. (2022). Diverse heliorhodopsins detected via functional metagenomics in freshwater Actinobacteria, Chloroflexi and Archaea. Env*iron Microbiol, 24(1)*, 110-121. doi:10.1111/1462-2920.15890

Chisti, Y. (2008). Biodiesel from microalgae beats bioethanol. Tre*nds Biotechnol, 26(3)*, 126-131. doi:10.1016/j.tibtech.2007.12.002

Chukhutsina, V. U., Fristedt, R., Morosinotto, T., & Croce, R. (2017). Photoprotection strategies of the alga Nannochloropsis gaditana. Bioc*him Biophys Acta Bioenerg, 1858(7),* 544-552. doi:10.1016/j.bbabio.2017.05.003

Dang, K. V., Plet, J., Tolleter, D., Jokel, M., Cuiné, S., Carrier, P., . . . Peltier, G. (2014). Combined increases in mitochondrial cooperation and oxygen photoreduction compensate for deficiency in cyclic electron flow in Chlamydomonas reinhardtii. Plan*t Cell, 26(7),* 3036-3050. doi:10.1105/tpc.114.126375

De Smet, I., Voss, U., Jürgens, G., & Beeckman, T. (2009). Receptor-like kinases shape the plant. Nat *Cell Biol, 11(10)*, 1166-1173. doi:10.1038/ncb1009-1166

Ebrahiminezhad, A., Rasoul-Amini, S., Ghoshoon, M. B., & Ghasemi, Y. (2014). Chlorella vulgaris, a novel microalgal source for l-asparaginase production. Bioc*atalysis and Agricultural Biotechnology, 3(2),* 214-217. doi:https://doi.org/10.1016/j.bcab.2013.10.005

Finazzi, G., Rappaport, F., Furia, A., Fleischmann, M., Rochaix, J. D., Zito, F., & Forti, G. (2002). Involvement of state transitions in the switch between linear and cyclic electron flow in Chlamydomonas reinhardtii. EMBO *Rep, 3(3),* 280-285. doi:10.1093/embo-reports/kvf047

Fleischmann, M. M., Ravanel, S., Delosme, R., Olive, J., Zito, F., Wollman, F. A., & Rochaix, J. D. (1999). Isolation and characterization of photoautotrophic mutants of Chlamydomonas reinhardtii deficient in state transition. Jour*nal of Biological Chemistry, 274(43)*. doi:10.1074/jbc.274.43.30987

Gentleman, R. C., Carey, V. J., Bates, D. M., Bolstad, B., Dettling, M., Dudoit, S., . . . Zhang, J. (2004). Bioconductor: open software development for computational biology and bioinformatics. Geno*me Biol, 5(10)*, R80. doi:10.1186/gb-2004-5-10-r80

Girolomoni, L., Bellamoli, F., Valbuena, G., Perozeni, F., D'Andrea, C., Cerullo, G., . . . Ballottari, M. (2020). Evolutionary divergence of photoprotection in the green algal lineage: a plant-like violaxanthin de-epoxidase enzyme activates the xanthophyll cycle in the green algaChlorella vulgarismodulating photoprotection. New *Phytologist, 228(1),* 136-150. doi:10.1111/nph.16674

Goehring, A. S., Rivers, D. M., & Sprague, G. F. (2003). Urmylation: a ubiquitin-like pathway that functions during invasive growth and budding in yeast. Mol *Biol Cell, 14(11)*, 4329-4341. doi:10.1091/mbc.e03-02-0079

Gordillo, F. J., Jiménez, C., Chavarría, J., & Xavier Niell, F. (2001). Photosynthetic acclimation to photon irradiance and its relation to chlorophyll fluorescence and carbon assimilation in the halotolerant green alga Dunaliella viridis. Phot*osynth Res, 68(3),* 225-235. doi:10.1023/A:1012969324756

Guarnieri, M. T., Nag, A., Yang, S., & Pienkos, P. T. (2013). Proteomic analysis of Chlorella vulgaris: potential targets for enhanced lipid accumulation. J Pr*oteomics, 93, 24*5-253. doi:10.1016/j.jprot.2013.05.025

Houille-Vernes, L., Rappaport, F., Wollman, F. A., Alric, J., & Johnson, X. (2011). Plastid terminal oxidase 2 (PTOX2) is the major oxidase involved in chlororespiration in Chlamydomonas. Proc *Natl Acad Sci U S A, 108(51)*, 20820-20825. doi:10.1073/pnas.1110518109

Johnson, X., & Alric, J. (2013). Central carbon metabolism and electron transport in Chlamydomonas reinhardtii: metabolic constraints for carbon partitioning between oil and starch. Euka*ryot Cell, 12(6),* 776-793. doi:10.1128/EC.00318-12

Juneja, A., Chaplen, F., & Murthy, G. (2016). Genome scale metabolic reconstruction of Chlorella variabilis for exploring its metabolic potential for biofuels. Bior*esource Technology, 213, 10*3-110. doi:10.1016/j.biortech.2016.02.118

Kedem, I., Milrad, Y., Kaplan, A., & Yacoby, I. (2021). Juggling Lightning: How Chlorella ohadii handles extreme energy inputs without damage. Phot*osynthesis Research, 147(3),* 329-344. doi:10.1007/s11120-020-00809-9

Klein, M., & Papenbrock, J. (2004). The multi-protein family of Arabidopsis sulphotransferases and their relatives in other plant species. J Ex*p Bot, 55(404*), 1809-1820. doi:10.1093/jxb/erh183

Kovalev, K., Volkov, D., Astashkin, R., Alekseev, A., Gushchin, I., Haro-Moreno, J. M., . . . Gordeliy, V. (2020). High-resolution structural insights into the heliorhodopsin family. Proc *Natl Acad Sci U S A, 117(8),* 4131-4141. doi:10.1073/pnas.1915888117

Koyande, A., Chew, K., Rambabu, K., Tao, Y., Chu, D., & Show, P. (2019). Microalgae: A potential alternative to health supplementation for humans. Food *Science and Human Wellness, 8(1),* 16-24. doi:10.1016/j.fshw.2019.03.001

Kuhlgert, S., Austic, G., Zegarac, R., Osei-Bonsu, I., Hoh, D., Chilvers, M., . . . Kramer, D. (2016). MultispeQ Beta: a tool for large-scale plant phenotyping connected to the open PhotosynQ network. Roya*l Society Open Science, 3(10)*. doi:10.1098/rsos.160592

Lange, P. R., Geserick, C., Tischendorf, G., & Zrenner, R. (2008). Functions of chloroplastic adenylate kinases in Arabidopsis. Plan*t Physiol, 146(2),* 492-504. doi:10.1104/pp.107.114702

Lavaud, J., Rousseau, B., & Etienne, A. (2004). General features of photoprotection by energy dissipation in planktonic diatoms (Bacillariophyceae). Jour*nal of Phycology, 40(1),* 130-137. doi:10.1046/j.1529-8817.2004.03026.x

Lemeille, S., Turkina, M. V., Vener, A. V., & Rochaix, J. D. (2010). Stt7-dependent phosphorylation during state transitions in the green alga Chlamydomonas reinhardtii. Mol *Cell Proteomics, 9(6),* 1281-1295. doi:10.1074/mcp.M000020-MCP201

Lepetit, B., Sturm, S., Rogato, A., Gruber, A., Sachse, M., Falciatore, A., . . . Lavaud, J. (2012). High light acclimation in the secondary plastids containing diatom Phaeodactylum tricornutum is triggered by the redox state of the plastoquinone pool. Plan*t Physiol. do*i:10.1104/pp.112.207811

Li, Y., Sommerfeld, M., Chen, F., & Hu, Q. (2010). Effect of photon flux densities on regulation of carotenogenesis and cell viability of Haematococcus pluvialis (Chlorophyceae). J App*l Phycol, 22(3),* 253-263. doi:10.1007/s10811-009-9453-6

Lin, M., & Oliver, D. J. (2008). The role of acetyl-coenzyme a synthetase in Arabidopsis. Plan*t Physiol, 147(4),* 1822-1829. doi:10.1104/pp.108.121269

Lum, K. K., Kim, J., & Lei, X. G. (2013). Dual potential of microalgae as a sustainable biofuel feedstock and animal feed. J An*im Sci Biotechnol, 4(1),* 53. doi:10.1186/2049-1891-4-53

Malkin, S., Armond, P. A., Mooney, H. A., & Fork, D. C. (1981). Photosystem II Photosynthetic Unit Sizes from Fluorescence Induction in Leaves : CORRELATION TO PHOTOSYNTHETIC CAPACITY. Plan*t Physiol, 67(3),* 570-579.

Martinis, J., Glauser, G., Valimareanu, S., Stettler, M., Zeeman, S. C., Yamamoto, H., . . . Kessler, F. (2014). ABC1K1/PGR6 kinase: a regulatory link between photosynthetic activity and chloroplast metabolism. Plan*t J, 77(2),* 269-283. doi:10.1111/tpj.12385

Mayr, S. J., Mendel, R. R., & Schwarz, G. (2021). Molybdenum cofactor biology, evolution and deficiency. Bioc*him Biophys Acta Mol Cell Res, 1868(1),* 118883. doi:10.1016/j.bbamcr.2020.118883

Nakai, Y., Harada, A., Hashiguchi, Y., Nakai, M., & Hayashi, H. (2012). Arabidopsis molybdopterin biosynthesis protein Cnx5 collaborates with the ubiquitin-like protein Urm11 in the thio-modification of tRNA. J Bi*ol Chem, 287(36)*, 30874-30884. doi:10.1074/jbc.M112.350090

Nawrocki, W. J., Santabarbara, S., Mosebach, L., Wollman, F. A., & Rappaport, F. (2016). State transitions redistribute rather than dissipate energy between the two photosystems in Chlamydomonas. Nat *Plants, 2, 16*031. doi:10.1038/nplants.2016.31

Niccolai, A., Zittelli, G., Rodolfi, L., Biondi, N., & Tredici, M. (2019). Microalgae of interest as food source: Biochemical composition and digestibility. Alga*l Research-Biomass Biofuels and Bioproducts, 42. do*i:10.1016/j.algal.2019.101617

Nimmy, M. S., Kumar, V., Suthanthiram, B., Subbaraya, U., Nagar, R., Bharadwaj, C., . . . Krishnamurthy, P. (2022). A Systematic Phylogenomic Classification of the Multidrug and Toxic Compound Extrusion Transporter Gene Family in Plants. Fron*t Plant Sci, 13, 77*4885. doi:10.3389/fpls.2022.774885

Niyogi, K. K. (2000). Safety valves for photosynthesis. Curr*ent Opinion in Plant Biology, 3(6),* 455-460. doi:http://dx.doi.org/10.1016/S1369-5266(00)00113-8

Ohara, K., Sasaki, K., & Yazaki, K. (2010). Two solanesyl diphosphate synthases with different subcellular localizations and their respective physiological roles in Oryza sativa. J Ex*p Bot, 61(10)*, 2683-2692. doi:10.1093/jxb/erq103

Pan, X., Eathiraj, S., Munson, M., & Lambright, D. G. (2006). TBC-domain GAPs for Rab GTPases accelerate GTP hydrolysis by a dual-finger mechanism. Natu*re, 442(710*0), 303-306. doi:10.1038/nature04847

Peers, G., Truong, T. B., Ostendorf, E., Busch, A., Elrad, D., Grossman, A. R., . . . Niyogi, K. K. (2009). An ancient light-harvesting protein is critical for the regulation of algal photosynthesis. Natu*re, 462(727*2), 518-521. doi:10.1038/nature08587

Perez-Riverol, Y., Bai, J., Bandla, C., García-Seisdedos, D., Hewapathirana, S., Kamatchinathan, S., . . . Vizcaíno, J. A. (2022). The PRIDE database resources in 2022: a hub for mass spectrometry-based proteomics evidences. Nucle*ic Acids Res, 50(D1),* D543-D552. doi:10.1093/nar/gkab1038

Perozeni, F., Cazzaniga, S., Baier, T., Zanoni, F., Zoccatelli, G., Lauersen, K., . . . Ballottari, M. (2020). Turning a green alga red: engineering astaxanthin biosynthesis by intragenic pseudogene revival in Chlamydomonas reinhardtii. Plant *Biotechnology Journal, 18(10),* 2053-2067. doi:10.1111/pbi.13364

Pushkarev, A., Inoue, K., Larom, S., Flores-Uribe, J., Singh, M., Konno, M., . . . Béjà, O. (2018). A distinct abundant group of microbial rhodopsins discovered using functional metagenomics. Natur*e, 558(7711*), 595-599. doi:10.1038/s41586-018-0225-9

Rahman, F., Hassan, M., Rosli, R., Almousally, I., Hanano, A., & Murphy, D. J. (2018). Evolutionary and genomic analysis of the caleosin/peroxygenase (CLO/PXG) gene/protein families in the Viridiplantae. PLoS *One, 13(5),* e0196669. doi:10.1371/journal.pone.0196669

Randhir, A., Laird, D., Maker, G., Trengove, R., & Moheimani, N. (2020). Microalgae: A potential sustainable commercial source of sterols. Algal *Research-Biomass Biofuels and Bioproducts, 46. doi*:10.1016/j.algal.2019.101772

Rani, A., Saini, K. C., Bast, F., Mehariya, S., Bhatia, S. K., Lavecchia, R., & Zuorro, A. (2021). Microorganisms: A Potential Source of Bioactive Molecules for Antioxidant Applications. Molec*ules, 26(4).* doi:10.3390/molecules26041142

Rosch, C., Rossmann, M., & Weickert, S. (2019). Microalgae for integrated food and fuel production. Globa*l Change Biology Bioenergy, 11(1),* 326-334. doi:10.1111/gcbb.12579

Rumeau, D., Peltier, G., & Cournac, L. (2007). Chlororespiration and cyclic electron flow around PSI during photosynthesis and plant stress response. Plant*, cell & environment, 30(9),* 1041-1051.

Sarayloo, E., Tardu, M., Unlu, Y., Simsek, S., Cevahir, G., Erkey, C., & Kavakli, I. (2017). Understanding lipid metabolism in high-lipid-producing Chlorella vulgaris mutants at the genome-wide level. Algal *Research-Biomass Biofuels and Bioproducts, 28, 244*-252. doi:10.1016/j.algal.2017.11.009

Sathasivam, R., Radhakrishnan, R., Hashem, A., & Abd Allah, E. (2019). Microalgae metabolites: A rich source for food and medicine. Saudi *Journal of Biological Sciences, 26(4),* 709-722. doi:10.1016/j.sjbs.2017.11.003

Schmitz, J., Chowdhury, M. M., Hänzelmann, P., Nimtz, M., Lee, E. Y., Schindelin, H., & Leimkühler, S. (2008). The sulfurtransferase activity of Uba4 presents a link between ubiquitin-like protein conjugation and activation of sulfur carrier proteins. Bioch*emistry, 47(24),* 6479-6489. doi:10.1021/bi800477u

Schneider, A., Steinberger, I., Strissel, H., Kunz, H. H., Manavski, N., Meurer, J., . . . Leister, D. (2014). The Arabidopsis Tellurite resistance C protein together with ALB3 is involved in photosystem II protein synthesis. Plant *J, 78(2),* 344-356. doi:10.1111/tpj.12474

Schreiber, U., & Klughammer, C. (2009). New NADPH / 9-AA module for the DUAL-PAM-100 : Description , operation and examples of application. In (Vol. 2, pp. 1-13). PAM a*pplication Notes.*

*Ser*ra-Maia, R., Bernard, O., Goncalves, A., Bensalem, S., & Lopes, F. (2016). Influence of temperature on Chlorella vulgaris growth and mortality rates in a photobioreactor. Algal *Research-Biomass Biofuels and Bioproducts, 18, 352*-359. doi:10.1016/j.algal.2016.06.016

Shahbazi, M., Gilbert, M., Labouré, A.-M., & Kuntz, M. (2007). Dual role of the plastid terminal oxidase in tomato. Plant *physiology, 145(3),* 691-702.

Simicevic, J., & Deplancke, B. (2017). Transcription factor proteomics-Tools, applications, and challenges. Prote*omics, 17(3-4)*. doi:10.1002/pmic.201600317

Simicevic, J., Schmid, A. W., Gilardoni, P. A., Zoller, B., Raghav, S. K., Krier, I., . . . Deplancke, B. (2013). Absolute quantification of transcription factors during cellular differentiation using multiplexed targeted proteomics. Nat M*ethods, 10(6),* 570-576. doi:10.1038/nmeth.2441

Simionato, D., Sforza, E., Corteggiani Carpinelli, E., Bertucco, A., Giacometti, G. M., & Morosinotto, T. (2011). Acclimation of Nannochloropsis gaditana to different illumination regimes: effects on lipids accumulation. Biore*sour Technol, 102(10),* 6026-6032. doi:10.1016/j.biortech.2011.02.100

Smith, B. M., Morrissey, P. J., Guenther, J. E., Nemson, J. A., Harrison, M. A., Allen, J. F., & Melis, A. (1990). Response of the Photosynthetic Apparatus in Dunaliella salina (Green Algae) to Irradiance Stress. Plant *Physiol, 93(4), 1*433-1440.

Spaniol, B., Lang, J., Venn, B., Schake, L., Sommer, F., Mustas, M., . . . Schroda, M. (2022). Complexome profiling on the Chlamydomonas lpa2 mutant reveals insights into PSII biogenesis and new PSII associated proteins. J Exp *Bot, 73(1), 2*45-262. doi:10.1093/jxb/erab390

Supek, F., Bošnjak, M., Škunca, N., & Šmuc, T. (2011). REVIGO summarizes and visualizes long lists of gene ontology terms. PLoS O*ne, 6(7), e*21800. doi:10.1371/journal.pone.0021800

Tardif, M., Atteia, A., Specht, M., Cogne, G., Rolland, N., Brugière, S., . . . Cournac, L. (2012). PredAlgo: a new subcellular localization prediction tool dedicated to green algae. Mol Bi*ol Evol, 29(12),* 3625-3639. doi:10.1093/molbev/mss178

Toyoshima, M., Sakata, M., Ohnishi, K., Tokumaru, Y., Kato, Y., Tokutsu, R., . . . Shimizu, H. (2019). Targeted proteome analysis of microalgae under high-light conditions by optimized protein extraction of photosynthetic organisms. J Biosc*i Bioeng, 127(3), 3*94-402. doi:10.1016/j.jbiosc.2018.09.001

Treves, H., Raanan, H., Kedem, I., Murik, O., Keren, N., Zer, H., . . . Kaplan, A. (2016). The mechanisms whereby the green alga Chlorella ohadii, isolated from desert soil crust, exhibits unparalleled photodamage resistance. New Ph*ytol, 210(4), 1*229-1243. doi:10.1111/nph.13870

Treves, H., Siemiatkowska, B., Luzarowska, U., Murik, O., Fernandez-Pozo, N., Moraes, T. A., . . . Stitt, M. (2020). Multi-omics reveals mechanisms of total resistance to extreme illumination of a desert alga. Nat Pl*ants, 6(8), 1*031-1043. doi:10.1038/s41477-020-0729-9

Uhmeyer, A., Cecchin, M., Ballottari, M., & Wobbe, L. (2017). Impaired Mitochondrial Transcription Termination Disrupts the Stromal Redox Poise in Chlamydomonas. Plant *Physiol, 174(3), 1*399-1419. doi:10.1104/pp.16.00946

Vanlerberghe, G. (2013). Alternative Oxidase: A Mitochondrial Respiratory Pathway to Maintain Metabolic and Signaling Homeostasis during Abiotic and Biotic Stress in Plants. Intern*ational Journal of Molecular Sciences, 14(4), 6*805-6847. doi:10.3390/ijms14046805

Vecchi, V., Barera, S., Bassi, R., & Dall'Osto, L. (2020). Potential and Challenges of Improving Photosynthesis in Algae. Plants-*Basel, 9(1). d*oi:10.3390/plants9010067

Väremo, L., Nielsen, J., & Nookaew, I. (2013). Enriching the gene set analysis of genome-wide data by incorporating directionality of gene expression and combining statistical hypotheses and methods. Nucle*ic Acids Res, 41(8), 4*378-4391. doi:10.1093/nar/gkt111

Wakao, S., Shih, P. M., Guan, K., Schackwitz, W., Ye, J., Patel, D., . . . Niyogi, K. K. (2021). Discovery of photosynthesis genes through whole-genome sequencing of acetate-requiring mutants of Chlamydomonas reinhardtii. PLoS G*enet, 17(9), e*1009725. doi:10.1371/journal.pgen.1009725

Wang, Y., Stessman, D., & Spalding, M. (2015). The CO2 concentrating mechanism and photosynthetic carbon assimilation in limiting CO2: how Chlamydomonas works against the gradient. Plant *Journal, 82(3), 4*29-448. doi:10.1111/tpj.12829

Wei, N., Chamovitz, D. A., & Deng, X. W. (1994). Arabidopsis COP9 is a component of a novel signaling complex mediating light control of development. Cell, *78(1), 1*17-124. doi:10.1016/0092-8674(94)90578-9

Yamano, T., Miura, K., & Fukuzawa, H. (2008). Expression analysis of genes associated with the induction of the carbon-concentrating mechanism in Chlamydomonas reinhardtii. Plant *Physiol, 147(1), 3*40-354. doi:10.1104/pp.107.114652

Yang, W., Catalanotti, C., D'Adamo, S., Wittkopp, T. M., Ingram-Smith, C. J., Mackinder, L., . . . Posewitz, M. C. (2014). Alternative acetate production pathways in Chlamydomonas reinhardtii during dark anoxia and the dominant role of chloroplasts in fermentative acetate production. Plant *Cell, 26(11),* 4499-4518. doi:10.1105/tpc.114.129965

Zhu, S. H., & Green, B. R. (2010). Photoprotection in the diatom Thalassiosira pseudonana: role of LI818-like proteins in response to high light stress. Biochi*m Biophys Acta, 1797(8), 1*449-1457. doi:10.1016/j.bbabio.2010.04.003

Zuniga, C., Li, C., Huelsman, T., Levering, J., Zielinski, D., McConnell, B., . . . Zengler, K. (2016). Genome-Scale Metabolic Model for the Green Alga Chlorella vulgaris UTEX 395 Accurately Predicts Phenotypes under Autotrophic, Heterotrophic, and Mixotrophic Growth Conditions. Plant *Physiology, 172(1), 5*89-602. doi:10.1104/pp.16.00593

TABLES

Table 1. High-performance liquid chromatography analysis of pigment content in *C. vulgaris* cells grown in LL or in HL conditions.

	Chl	Chl a/b	Chl/Car	Neo	Vio	Anthera	Lut	Zea	β car	Car tot
LL	3.93	3.24	2.59	0.21	0.20	n.d.	0.89	n.d.	0.21	1.72
S.D.	*0.73*	*0.40*	*0.12*	*0.04*	*0.04*	---	*0.17*	---	*0.04*	*0.33*
HL	1.60**	4.19	1.01**	0.05**	0.14	0.04*	0.91	0.22**	0.21	1.63
S.D.	*0.05*	*0.84*	*0.01*	*0.00*	*0.01*	*0.02*	*0.03*	*0.02*	*0.02*	*0.05*

Anthera, antheraxanthin; β car, β carotene; Chl, chlorophyll; Car, carotenoids; HL, high light; LL, low light; N.d., not detectable Neo, neoxanthin; Vio, violaxanthin; Zea, zeaxanthin; Car tot: total carotenoids Chlorophyll and carotenoid contents are normalized to $1x10^7$ cells. Errors are reported as standard deviation (n = 4). *p < 0.05 or **p < 0.01 for HL vs. LL.

Table 2. Oxygen evolution and dark respiration. The light curves in Fig. 3A were fitted by hyperbolic functions to determine the photosynthetic parameters Pmax and half-saturation intensity.

	LL	**HL**
Pmax (μmol O_2 h^{-1} μg Chl^{-1})	64.68 ± 1.49	204.50 ± 5.92**
Half-saturation intensity (μmol photons m^{-2} s^{-1})	142.78 ± 6.50	509.39 ± 26.72**

Chl, chlorophyll; Half-saturation intensity, actinic light intensity at which the oxygen evolution rate is Pmax/2; HL, high light; LL, low light; Pmax, maximum light dependent net oxygen evolution rate. Dark respiration values normalized on a cell or chlorophyll basis are reported for LL- and HL-acclimated cells. *p < 0.05 or **p < 0.01 for HL vs. LL

FIGURE LEGENDS

Figure 1. Functional antenna sizes of Photosystems I and II and the state transitions. A) Chlorophyll a fluorescence emission kinetics of whole cells grown in low light (LL) or high light (HL) treated with DCMU (representative of 3 independent biologic replicates), related with the light-harvesting efficiency of PSII. B) Kinetics of PSI reaction center oxidation followed by pump-probe differential absorption at 800 nm measured in whole cells treated with DCMU, methyl-viologen, and ascorbate (representative of 3 independent biologic replicates) as described in the Methods section. C, D) Chlorophyll a fluorescence emission spectra measured at 77K for cells grown in LL (C) or HL (D) in State 1 (S1) or State 2 (S2); S1 was induced in LL (~5 μmol m^2 s^{-1}) with 10 μm of DCMU to oxidize the plastoquinone pool while S2 was induced by adding 250 μM sodium azide to inhibit mitochondrial respiration and reduce the plastoquinone pool. E) Extent of State Transition retrieved from fluorescence emission spectra reported in C) and D) from the maximum fluorescence emission at 720 nm as (FS2-FS1)/FS2. Error bars are reported as standard deviations (n = 3). *p < 0.05 for HL vs. LL

Figure 2. Oxygen evolution and electrochromic shift measurements. A) Light curves of LL- and HL-acclimated cells measured as net light-dependent oxygen evolution rates at different actinic lights. Experimental data were fitted with hyperbolic functions, and fitting results are shown as dotted lines. B) ECS measurements at different actinic lights for LL and HL cells in the presence (dotted lines) or absence (solid lines) of DCMU. C) Percentage of residual ECS upon DCMU treatment compared to untreated cells; the residual ECS may be related to cyclic electron transport. Data are the means of three biological replicates with error bars showing the standard deviations. ECS, electrochromic shift; HL, high light; LL, low light. *p < 0.05 or **p < 0.01 for HL vs. LL.

Figure 3. Photosynthetic parameters and NAD(P)H reduction rates. A) Maximal PSI activity (P700 oxidation) on a chlorophyll basis measured in LL- or HL-acclimated cells. B, C) PSII quantum yield (B) and 1-qL (reduced Q_A fraction, C), at different actinic light intensities for LL- or HL-acclimated cells. D) NPQ kinetics measured upon exposure of dark-adapted LL or HL cells to 1400 μmol m-2 s-1 actinic light for 8 min followed by dark relaxation. E) NPQ values at the end of the actinic light exposure as described in D) at different actinic light intensities for LL- or HL-acclimated cells (see Fig. S1 for more details). Data are means of three biological replicates with error bars showing the standard deviations. F) Kinetics of NAD(P)H fluorescence emission measured on dark-adapted LL or HL cells: actinic light (1400 μmol m^{-2} s^{-1}) was turned on after 20 s and turned off at 120 s. NAD(P)H fluorescence emission kinetics were normalized to the initial rise upon exposure to actinic light. HL, high light; LL, low light; NPQ, non-photochemical quenching. *p < 0.05 or **p < 0.01 for HL vs. LL.

Figure 4. Dark respiration of Chlorella vulgaris cells grown in LL or HL conditions. Dark respiration is reported as total dark respiration measured in absence of inhibitors (TOT) and the relative contribution of cytochrome (CITOCHROME) and alternative respiration (ALTERNATIVE) measured in presence of SHAM or mixothiazol, inhibiting respectively AOX and Complex III. Data are the means of three biological replicates

with error bars showing the standard deviations. HL, high light; LL, low light. *p < 0.05 or **p < 0.01 for HL vs. LL.

Figure 5. Analysis of differentially expressed proteins in HL- vs. LL-acclimated *Chlorella vulgaris* cells. A) PCA analysis of the replicates analyzed for HL and LL samples. B) Volcano Plots Representing the Systems Response Profiles. For each protein, the protein expression change (calculated as the log2 fold change) is plotted on the x-axis and the statistical significance (proportional to the negative log10-adjusted p-value) is plotted on the y-axis. Yellow and cyan dots highlight proteins that are statistically significantly up- and down-regulated, respectively (FDR-adjusted p < 0.05). C) Top 10 proteins upregulated or downregulated in HL vs. LL by log2 fold-change. FDR, false discovery rate; HL, high light; LL, low light; PCA, principal component analysis. D) Gene-set enrichment analysis (GSEA) performed on GO terms. Gene set statistics shown for significantly affected gene sets (fdr-adjusted p-value < 0.05). Note that only downregulated gene-sets were identified as significantly enriched in the GSEA.

Figure 6. Schematic model of cell metabolism adaptation to LL or HL conditions. The model represented is based on the physiologic measurements on photosynthetic activity and mitochondrial respiration and on proteomic analysis described in this work. Red, blue and black colors indicate metabolic flows or metabolite/protein concentrations estimated respectively as upregulated, downregulated or unchanged in HL vs. LL cells. The metabolic pathways are indicated in italic. The metabolic flux here estimated as upregulated, downregulated or unchanged derive from a model based on enzyme concentration (proteins determined as differentially expressed by proteomic analysis are reported in red or blue for upregulated or downregulated proteins). Only in the case of photosynthetic electron flow, cyclic electron flow (CEF) and mitochondrial respiration the estimated fluxes derived from experimental data. Background of the figure representing the intracellular structure was obtained with BioRender software. PPI: peptidyl-proyl isomerase; NR: nitrate reductase; AOX: alternative oxidase; PSI/II: Photosystem I/II; LHCI/II: Light Harvesting Complex I/II; TF: transcription factor; ACS: acetyl-CoA synthase, PAT: phosphate acetyltransferase; Chl: chlorophyll; CCM: carbon concentrating mechanism; Glu: glutamate; PTOX: Plastid Terminal Oxidase; CBB: Calvin-Benson-Basham cycle; Adenyklate-K: adenylate kinase; Cytb6f; cytochrome b6f.

FIGURES

Figure 1

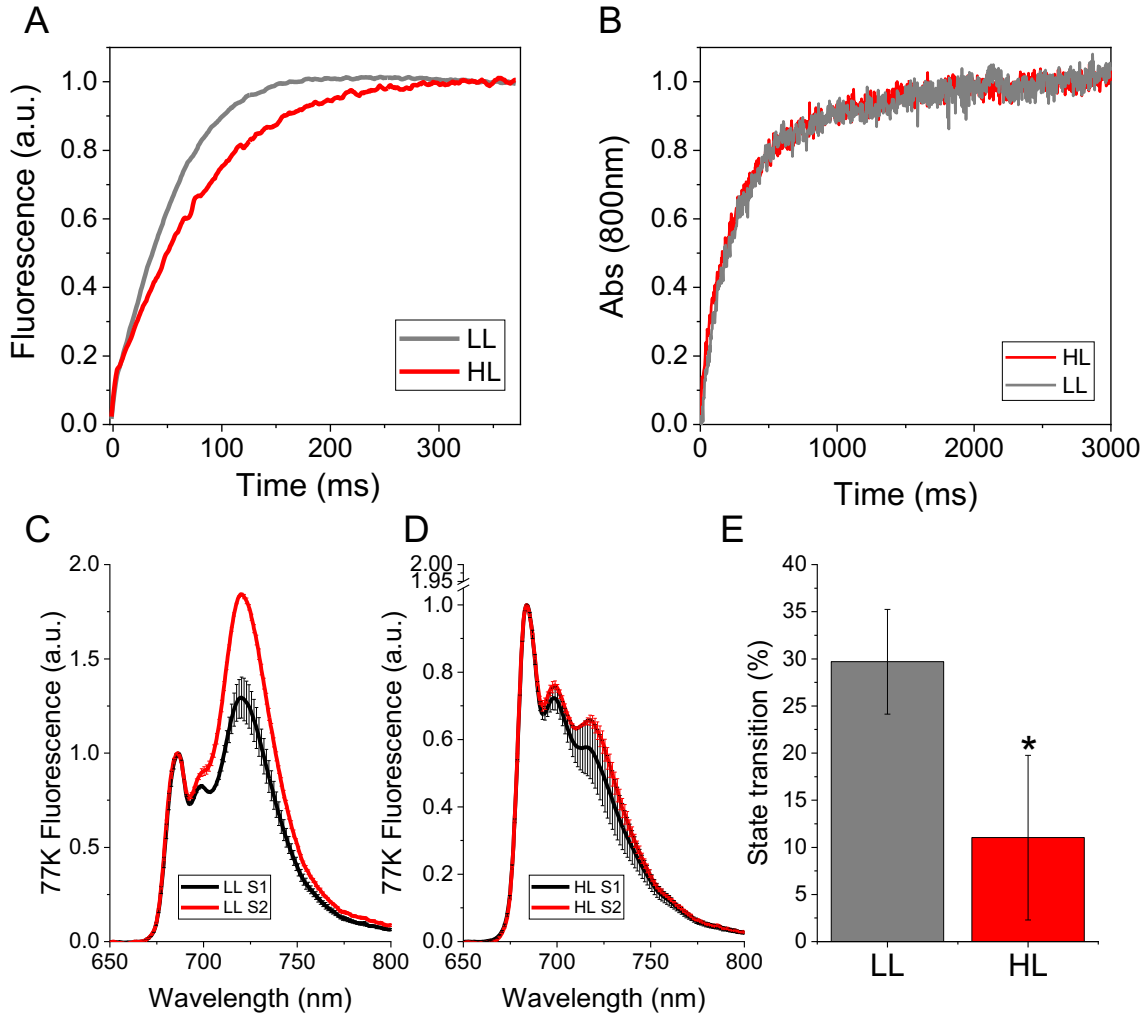

Figure 1. Functional antenna sizes of Photosystems I and II and the state transitions. A) Chlorophyll a fluorescence emission kinetics of whole cells grown in low light (LL) or high light (HL) treated with DCMU (representative of 3 independent biologic replicates), related with the light-harvesting efficiency of PSII. B) Kinetics of PSI reaction center oxidation followed by pump-probe differential absorption at 800 nm measured in whole cells treated with DCMU, methyl-viologen, and ascorbate (representative of 3 independent biologic replicates) as described in the Methods section. C, D) Chlorophyll a fluorescence emission spectra measured at 77K for cells grown in LL (C) or HL (D) in State 1 (S1) or State 2 (S2); S1 was induced in LL (~5 µmol m^2 s^{-1}) with 10 µm of DCMU to oxidize the plastoquinone pool while S2 was induced by adding 250 µM sodium azide to inhibit mitochondrial respiration and reduce the plastoquinone pool. E) Extent of State Transition retrieved from fluorescence emission spectra reported in C) and D) from the maximum fluorescence emission at 720 nm as (FS2-FS1)/FS2. Error bars are reported as standard deviations (n = 3). *$p < 0.05$ for HL vs. LL.

Figure 2

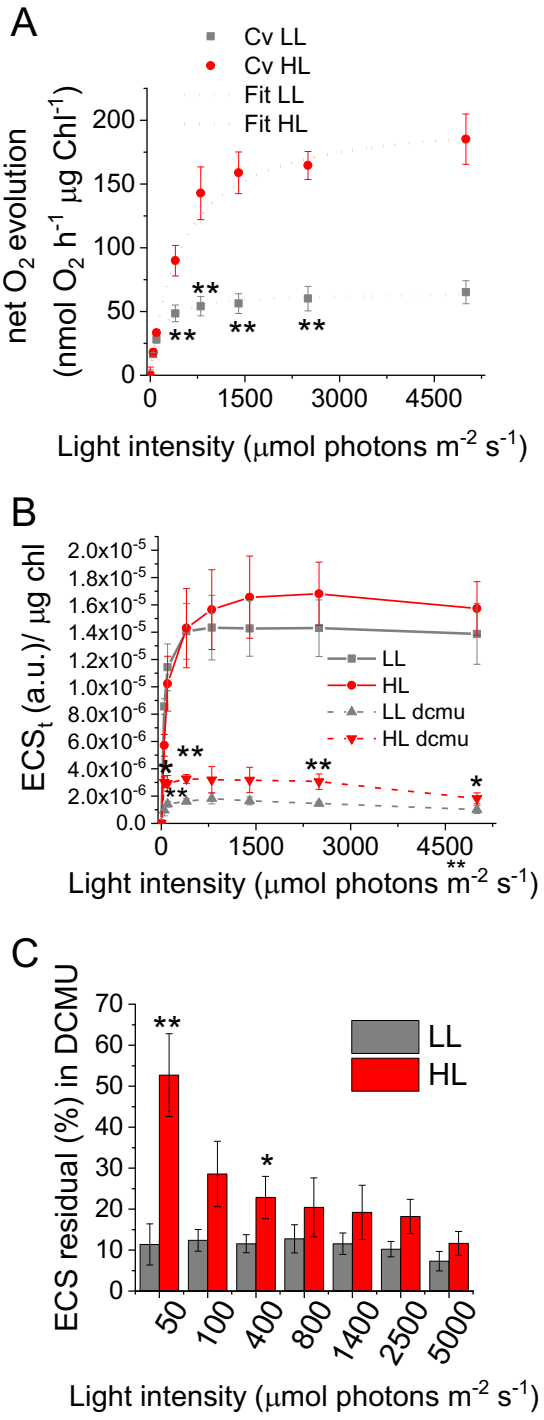

Figure 2. Oxygen evolution and electrochromic shift measurements. A) Light curves of LL- and HL-acclimated cells measured as net light-dependent oxygen evolution rates at different actinic lights. Experimental data were fitted with hyperbolic functions, and fitting results are shown as dotted lines. B) ECS measurements at different actinic lights for LL and HL cells in the presence (dotted lines) or absence (solid lines) of DCMU. C) Percentage of residual ECS upon DCMU treatment compared to untreated cells; the residual ECS may be related to cyclic electron transport. Data are the means of three biological replicates with error bars showing the standard deviations. ECS, electrochromic shift; HL, high light; LL, low light. *$p < 0.05$ or **$p < 0.01$ for HL vs. LL.

Figure 3

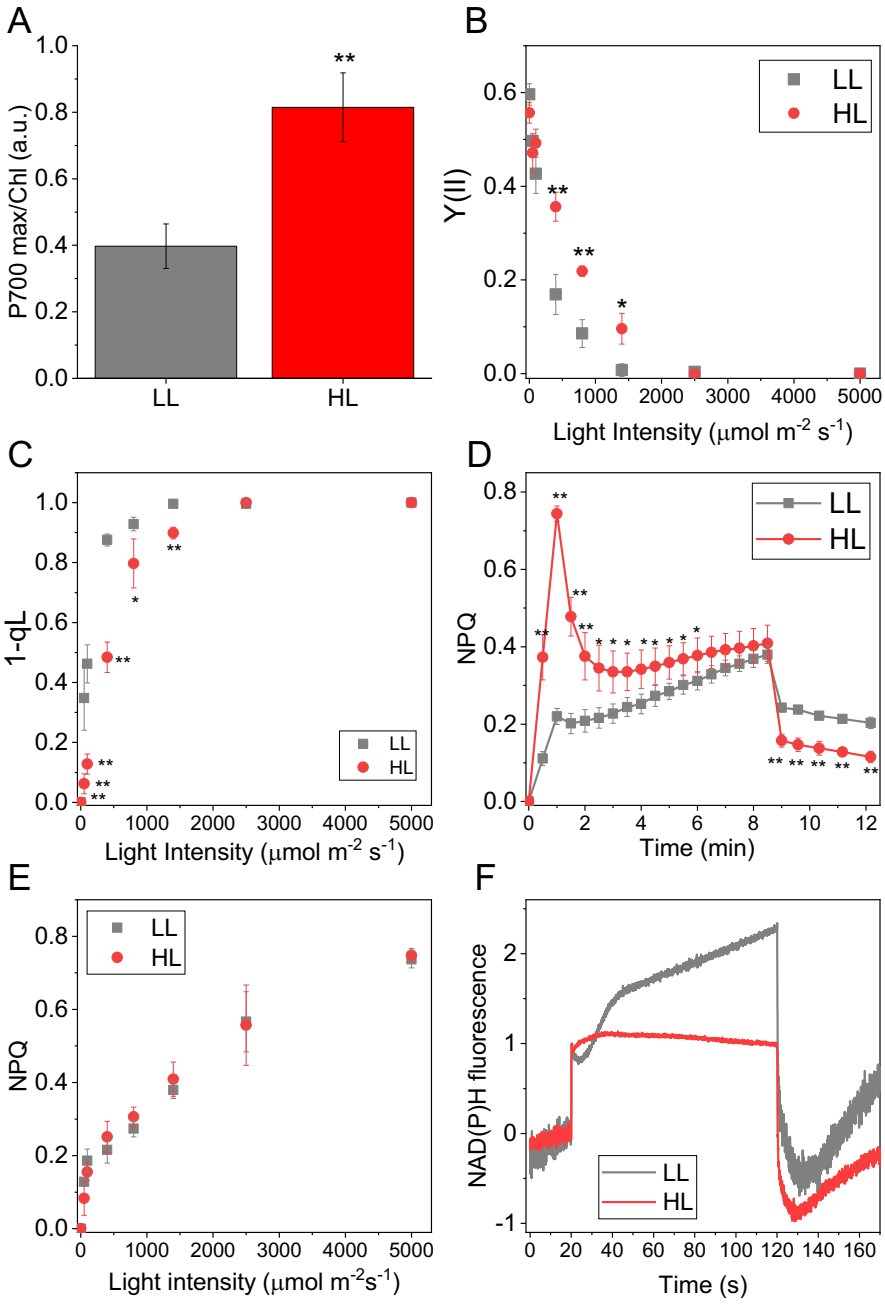

Figure 3. Photosynthetic parameters and NAD(P)H reduction rates. A) Maximal PSI activity (P700 oxidation) on a chlorophyll basis measured in LL- or HL-acclimated cells. B, C) PSII quantum yield (B) and 1-qL (reduced Q_A fraction, C), at different actinic light intensities for LL- or HL-acclimated cells. D) NPQ kinetics measured upon exposure of dark-adapted LL or HL cells to 1400 µmol m-2 s-1 actinic light for 8 min followed by dark relaxation. E) NPQ values at the end of the actinic light exposure as described in D) at different actinic light intensities for LL- or HL-acclimated cells (see Fig. S1 for more details). Data are means of three biological replicates with error bars showing the standard deviations. F) Kinetics of NAD(P)H fluorescence emission measured on dark-adapted LL or HL cells: actinic light (1400 µmol m^{-2} s^{-1}) was turned on after 20 s and turned off at 120 s. NAD(P)H fluorescence emission kinetics were normalized to the initial rise upon exposure to actinic light. HL, high light; LL, low light; NPQ, non-photochemical quenching. *p < 0.05 or **p < 0.01 for HL vs. LL.

Figure 4

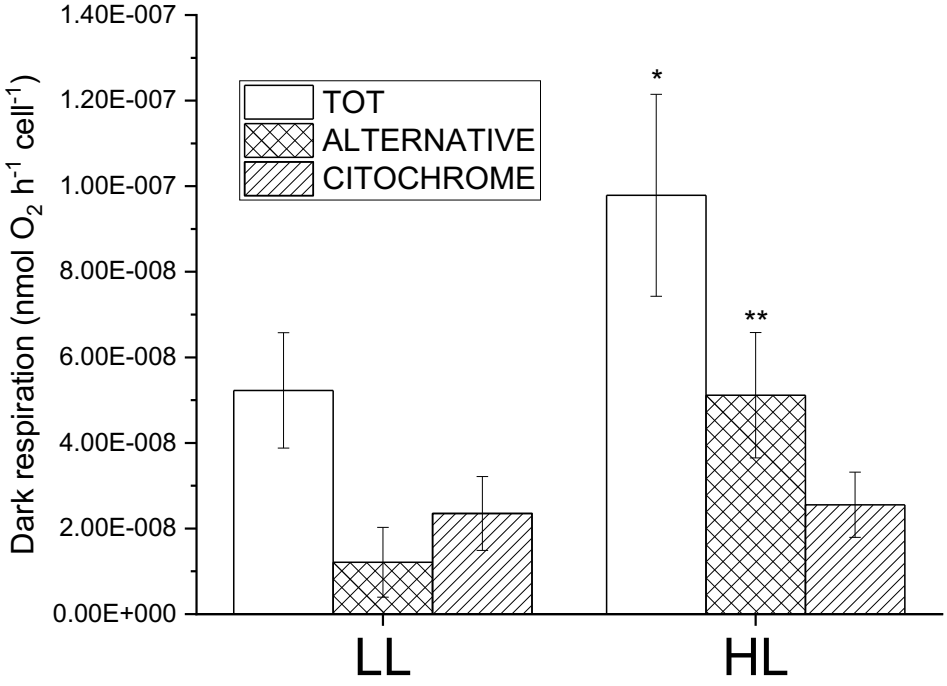

Figure 4 Dark respiration of Chlorella vulgaris cells grown in LL or HL conditions. Dark respiration is reported as total dark respiration measured in absence of inhibitors (TOT) and the relative contribution of cytochrome (CITOCHROME) and alternative respiration (ALTERNATIVE) measured in presence of SHAM or mixothiazol, inhibiting respectively AOX and Complex III. Data are the means of three biological replicates with error bars showing the standard deviations. HL, high light; LL, low light. *$p < 0.05$ or **$p < 0.01$ for HL vs. LL.

Figure 5

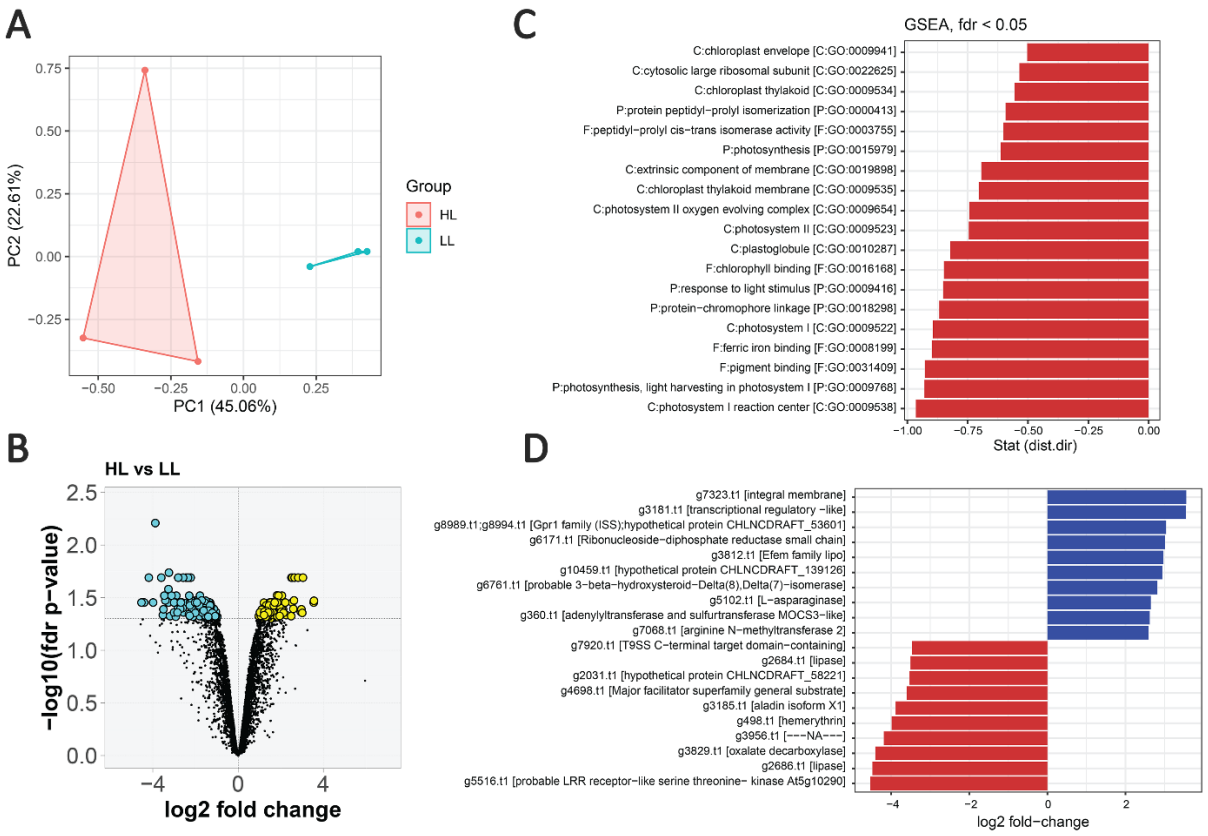

Figure 5. Analysis of differentially expressed proteins in HL- vs. LL-acclimated *Chlorella vulgaris* cells. a) PCA analysis of the replicates analyzed for HL and LL samples. b) Volcano plots representing the systems response profiles. For each protein, the protein expression change (calculated as the log2 fold change) is plotted on the x-axis and the statistical significance (proportional to the negative log10-adjusted p-value) is plotted on the y-axis. Yellow and cyan dots highlight proteins that are statistically significantly up- and down-regulated, respectively (FDR-adjusted $p < 0.05$). C) Top 10 proteins upregulated or downregulated in HL vs. LL by log2 fold-change. FDR, false discovery rate; HL, high light; LL, low light; PCA, principal component analysis. D) Gene-set enrichment analysis (GSEA) performed on GO terms. Gene set statistics shown for significantly affected gene sets (fdr-adjusted p-value < 0.05). Note that only downregulated gene-sets were identified as significantly enriched in the GSEA.

Figure 6

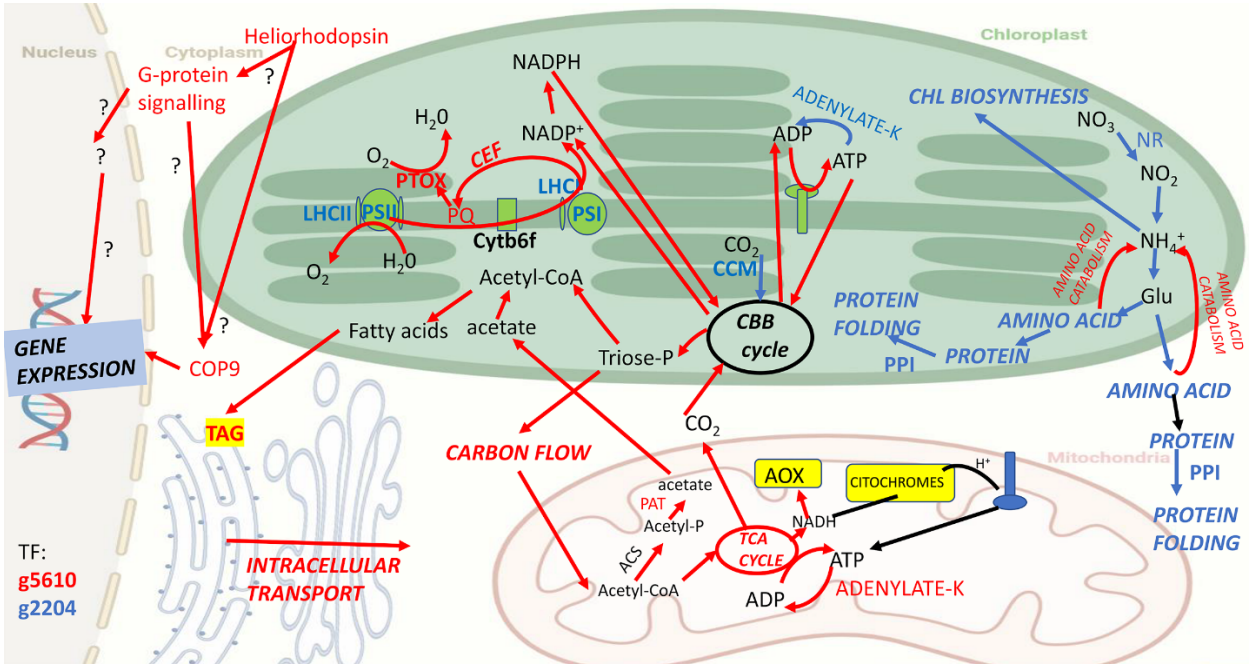

Figure 6. Schematic model of cell metabolism adaptation to LL or HL conditions. The model represented is based on the physiologic measurements on photosynthetic activity and mitochondrial respiration and on proteomic analysis described in this work. Red, blue and black colors indicate metabolic flows or metabolite/protein concentrations estimated respectively as upregulated, downregulated or unchanged in HL vs. LL cells. The metabolic pathways are indicated in italic. The metabolic flux here estimated as upregulated, downregulated or unchanged derive from a model based on enzyme concentration (proteins determined as differentially expressed by proteomic analysis are reported in red or blue for upregulated or downregulated proteins). Only in the case of photosynthetic electron flow, cyclic electron flow (CEF) and mitochondrial respiration the estimated fluxes derived from experimental data. Background of the figure representing the intracellular structure was obtained with BioRender software. PPI: peptidyl-proyl isomerase; NR: nitrate reductase; AOX: alternative oxidase; PSI/II: Photosystem I/II; LHCI/II: Light Harvesting Complex I/II; TF: transcription factor; ACS: acetyl-CoA synthase, PAT: phosphate acetyltransferase; Chl: chlorophyll; CCM: carbon concentrating mechanism; Glu: glutamate; PTOX: Plastid Terminal Oxidase; CBB: Calvin-Benson-Basham cycle; Adenyklate-K: adenylate kinase; Cytb6f; cytochrome b6f.